Full characterization of GPCR monomer–dimer dynamic equilibrium by single molecule imaging

Rinshi S. Kasai,[1] Kenichi G. N. Suzuki,[2] Eric R. Prossnitz,[3] Ikuko Koyama-Honda,[1] Chieko Nakada,[1] Takahiro K. Fujiwara,[1] and Akihiro Kusumi[1]

[1]Membrane Mechanisms Project, International Cooperative Research Project (ICORP), and [2]Precursory Research for Embryonic Science and Technology (PRESTO), Japan Science and Technology Agency, Institute for Integrated Cell-Material Sciences (iCeMS), and Institute for Frontier Medical Sciences, Kyoto University, Shougoin, Kyoto 606-8507, Japan
[3]Department of Cell Biology and Physiology, University of New Mexico Health Science Center, Albuquerque, NM 87131

Receptor dimerization is important for many signaling pathways. However, the monomer–dimer equilibrium has never been fully characterized for any receptor with a 2D equilibrium constant as well as association/dissociation rate constants (termed super-quantification). Here, we determined the dynamic equilibrium for the N-formyl peptide receptor (FPR), a chemoattractant G protein–coupled receptor (GPCR), in live cells at 37°C by developing a single fluorescent-molecule imaging method. Both before and after liganding, the dimer–monomer 2D equilibrium is unchanged, giving an equilibrium constant of 3.6 copies/µm², with a dissociation and 2D association rate constant of 11.0 s⁻¹ and 3.1 copies/µm²s⁻¹, respectively. At physiological expression levels of ∼2.1 receptor copies/µm² (∼6,000 copies/cell), monomers continually convert into dimers every 150 ms, dimers dissociate into monomers in 91 ms, and at any moment, 2,500 and 3,500 receptor molecules participate in transient dimers and monomers, respectively. Not only do FPR dimers fall apart rapidly, but FPR monomers also convert into dimers very quickly.

Introduction

Receptor dimerization is often the first step for induction of intracellular signals after ligand binding (Weiss and Schlessinger, 1998; Wu et al., 2004). Furthermore, even in the absence of extracellular stimulation, many receptors have been proposed to form dimers, including the EGF receptor (Chung et al., 2010) and several G protein–coupled receptors (GPCRs; Harding et al., 2009; for reviews see Fotiadis et al., 2006; Panetta and Greenwood, 2008; Simpson et al., 2010). These preformed dimers were found to facilitate the formation of dimers of engaged receptors, accelerating or decelerating the rate at which downstream signals are activated (Han et al., 2009; Chung et al., 2010). In addition, many downstream signaling molecules located on the cytoplasmic surface of the plasma membrane might also be activated via dimerization, as seen in the autophosphorylation of Raf caused by Ras dimerization (Inouye et al., 2000).

However, the densities of receptor monomers and dimers and the dimer dissociation equilibrium constant in the membrane

plane, particularly in living cells, have never been determined. The lack of such quantitative evaluations severely limits our ability to correctly predict time-dependent changes of the intensities and the spatial spreads of downstream signals. Therefore, in order to advance our fundamental mechanistic understanding of signal transduction in and on the plasma membrane, a means to accomplish exact quantification by accurately counting the number densities of receptors and obtaining a full description of the dynamic equilibrium between receptor monomers and dimers must be developed. The latter includes (a) the 2D equilibrium dimer dissociation constant (2D-K_D), (b) the rate constant for dimer formation (monomer association; k_a), and (c) the rate constant for dimer dissociation (k_d). Only after these parameters are accurately evaluated can research using quantitative modeling be initiated, which is absolutely required for our understanding of receptor-triggered signal transduction in the plasma membrane and may aid in our understanding of why receptor dimerization became a step in this signal transduction pathway (Gurevich and Gurevich, 2008).

Correspondence to Akihiro Kusumi: akusumi@frontier.kyoto-u.ac.jp

Abbreviations used in this paper: ACP, acyl carrier protein; BAR, β2-adrenergic receptor; BiFC, bimolecular fluorescence complementation; DOPE, L-α-dioleoyl-phosphatidylethanolamine; FM, fluorescent molecule; FPR, N-formyl peptide receptor; GPCR, G protein–coupled receptor; mGFP, monomeric GFP; NDDS, number density of distinguishable spots; TIRF, total internal reflection fluorescence; WT, wild type.

In the present study, by developing a new method and theoretical framework, we for the first time succeeded in fully characterizing the dynamic monomer–dimer equilibrium of a receptor in the plasma membrane. As an important paradigm, we used the *N*-formyl peptide receptor (FPR), a family A GPCR, which is largely responsible for triggering the chemotaxis of neutrophils and other immune cells (Snyderman and Pike, 1984; Prossnitz and Ye, 1997; Panaro et al., 2006).

Within the GPCR field, the questions of whether dimers exist under physiological conditions and whether dimerization is necessary for the function of a particular GPCR have been the subjects of extensive controversy (Meyer et al., 2006; Whorton et al., 2007). The existence of dimers has been quite well established among the family C GPCRs, including homodimers of metabotropic glutamate receptor 1 (Kunishima et al., 2000) and heterodimers of GABA$_B$ receptor (Jones et al., 1998; Kaupmann et al., 1998; White et al., 1998), for which dimers are proposed to be essential to function. However, evidence for dimers among the largest family A group of GPCRs is mixed; although noncovalent dimers of family A GPCRs have been detected in cells by biophysical and biochemical methods (Angers et al., 2000; Goin and Nathanson, 2006; Harding et al., 2009), questions have been raised (James et al., 2006; Meyer et al., 2006). For example, James et al. (2006) pointed out that because many of the experiments for detecting noncovalent GPCR dimers have been performed under overexpression conditions or in the presence of high concentrations of the receptor molecules in vitro, the actual amounts of dimers might be very limited under physiological conditions. Prominently, they arrived at the important conclusion that a prototypical GPCR, the β2-adrenergic receptor (BAR), does not form dimers, contrary to previous studies (Angers et al., 2000; Mercier et al., 2002). Meanwhile, the dimer lifetime of 0.7 s (23°C), as recently determined for the first time for a GPCR, the M1 muscarinic receptor, might have made the detection of dimers difficult (Hern et al., 2010; Lambert, 2010).

The function of family A GPCR dimers and oligomers was proposed (see, for example, Wenzel-Seifert and Seifert [2003] for FPR and Hebert et al. [1996] and Salahpour et al. [2004] for BAR), but it is generally held that dimer or oligomer formation is not essential for their function (Ernst et al., 2007; Whorton et al., 2007, 2008). Although GPCR dimerization is an actively studied area in GPCR research, available techniques have not unequivocally differentiated between GPCR monomers and dimers in the plasma membrane of living cells, and in addition have failed to reach unequivocal conclusions on the functions of prospective dimers for many GPCRs.

The best way to resolve this controversy regarding the existence of GPCR dimers would be to fully characterize the monomer–dimer equilibrium by explicitly determining the 2D-K_D, k_a, and k_d in living cells. In the present study, we determined these three critical parameters for FPR, for the first time ever for any membrane molecule, by developing a method for evaluating the numbers of monomers and dimers of FPR (at various expression levels of ~0.3–2.5 copies/μm^2 or ~840–7,000 copies/cell for a spherical cell of 15 μm radius) encompassing physiological expression levels (2.1 FPR copies/μm^2 or

6,000 copies/cell; Tennenberg et al., 1988) in the plasma membrane of live cells at 37°C.

Such exact quantification was made possible by using single fluorescent molecule (FM) imaging (Koyama-Honda et al., 2005; Jaqaman et al., 2008; Triller and Choquet, 2008) as well as by explicitly including the fraction of molecules that actually fluoresce (labeling efficiency), *f*, in the evaluation protocol (for example, even for mature GFP, large fractions of molecules can be nonfluorescent; without knowing *f*, even if one employs single FM imaging, one could not determine the fractions of monomers, dimers, etc.). In addition, molecular-level interactions were confirmed by bimolecular fluorescence complementation (BiFC; Hu et al., 2002), which was observed for the first time at the level of single molecules.

Accordingly, we fully characterized the monomer–dimer dynamic equilibrium of FPR expressed in living cells, at a level we termed "super-quantification," as the following. The 2D-K_D at 37°C was determined to be 3.6 copies/μm^2, with a dimer lifetime of 91 ms (k_d of 11.0 s^{-1}) and k_a of 3.1 [copies/ μm^2]$^{-1}$s^{-1}. Under physiological expression conditions of 2.1 FPR copies/μm^2 (~6,000 copies/cell), monomers are continually converted into dimers every 150 ms. Dimers are dissociated into monomers in 91 ms, and on average, 41% of FPR exists as transient dimers; i.e., 2,500 FPR molecules exist in dimers (which equals 1,250 dimers) and 3,500 molecules are in monomers (59%) at any moment. Furthermore, we found that ligand addition does not affect dimer–monomer equilibrium.

Such an exact description of receptor monomer–dimer equilibrium has never been achieved, and opens the way for quantitative modeling studies. This newly developed method can be applied to determine the monomer and dimer concentrations of any cell-surface receptor, including other GPCRs, and thus will greatly help to advance our fundamental understanding of signal transduction mechanisms.

Results

Fluorescent-ligand labeling of FPR

An *N*-formyl hexa-amino-acid peptide (FP) was conjugated with the Alexa Fluor 594 dye at the sole amine group in the peptide, the ε-amine on the C-terminal lysine (the α-amine at the N terminus is formylated), at a precise 1:1 mol ratio (AlexaFP; Fig. 1 A; See Materials and methods, "Preparation of the formyl peptide…"). When this peptide probe was applied to the cell, the ligand-bound wild-type FPR (WT-FPR) became rapidly concentrated, probably at the internalization apparatuses in the plasma membrane as expected (see Fig. 8 C). Therefore, AlexaFP cannot be used to determine the FPR dimer fraction. To circumvent this problem, we first used a nonactivating mutant of FPR (D71A) expressed in CHO cells. This mutant binds the ligand with the same affinity as the WT-FPR (Fig. S2 and related text), but cannot activate G proteins (Prossnitz et al., 1999) and is neither phosphorylated nor internalized (Miettinen et al., 1999; Prossnitz et al., 1999). Furthermore, as described later (see Fig. 8 C), we found that the dimer fraction of WT-FPR before ligation, which we finally hoped to obtain, is the same
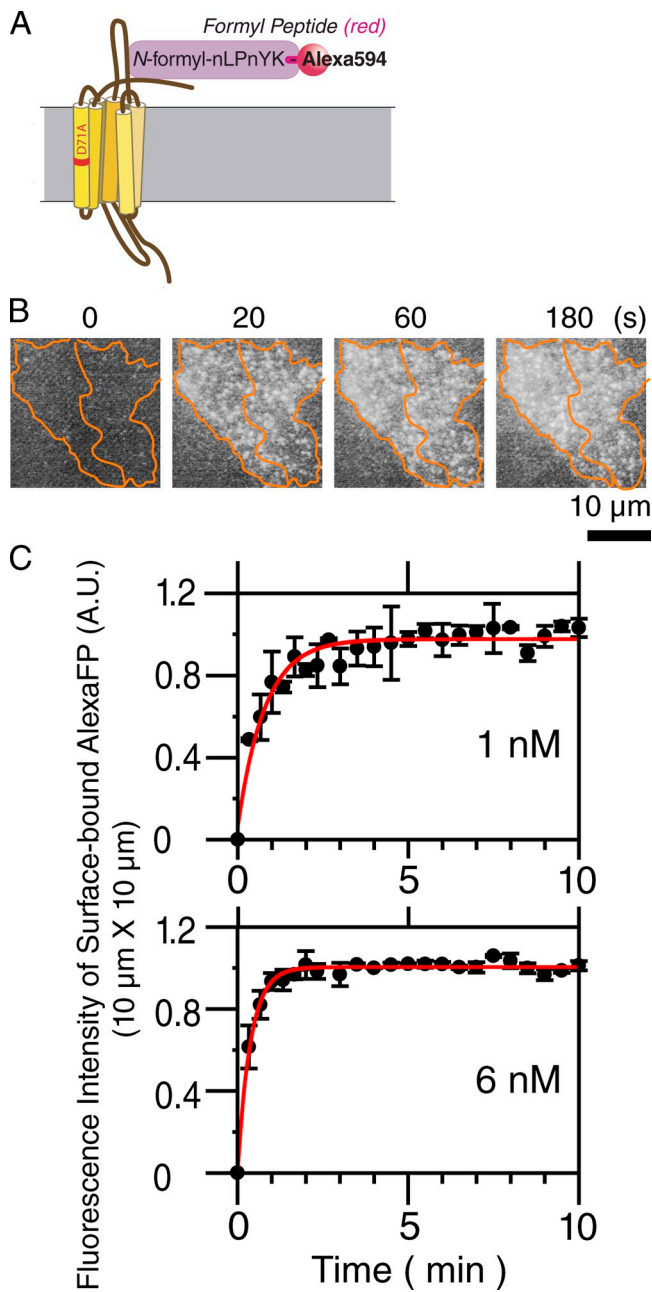
A Formyl Peptide (red)
N-formyl-nLPnYK—Alexa594

B 0   20   60   180 (s)

10 μm

C

Fluorescence Intensity of Surface-bound AlexaFP (A.U.)
(10 μm × 10 μm)

1 nM

6 nM

Time (min)

Figure 1. **Time needed to attain equilibrium for AlexaFP binding to D71A located on the bottom surface of live CHO cells.** (A) Schematic drawing of D71A bound by AlexaFP. n, norleucine. (B) A representative time series of TIRF images, observed at 0, 20, 60, and 180 s after applying 1 nM AlexFP. Orange lines indicate the perimeters of the two cells found in this view field. The punctate appearance is probably caused by the presence of dimers, incidentally overlapped monomers within the spatial resolution limit, and statistical variations. (C) Time-dependent increases in the fluorescence intensities of the surface-bound AlexaFP in the area of 10 × 10 μm, after applying 1 (top) and 6 nM (bottom) AlexaFP. The y axis is normalized using the saturation value for each concentration, but the absolute saturation value for the 1-nM experiment is ∼0.43× of that for the 6-nM experiment. Red curves show the best fit function $I(t) = C_N \{1 - \exp[-k[c]t]\}$ ([c], AlexaFP concentration; fitting parameters; $C_N = \sim1$; k, binding rate constant), with a k of 0.0076 ± 0.0017 $s^{-1}nM^{-1}$ (five independent determinations), yielding the exponential time constant for 6 nM AlexaFP of 22 ± 4.1 s. Note that each value determined in this paper is given as the mean ± standard error (error bars), and, in the case of the fitting parameters, the fitting error at the 68.3% confidence limit is given. This result clearly indicates that the ligand quickly enters the space between the bottom membrane and the coverslip, and that the AlexaFP

as the dimer fraction of D71A after (as well as before) ligation, which is experimentally observable. Therefore, we determined the monomer–dimer dynamic equilibrium of WT-FPR in the steady-state by observing the D71A mutant conjugated with AlexaFP. Finally, we determined the dimer–monomer equilibrium of WT-FPR right after the binding of the FP ligand (before the liganded receptors start assembling in clathrin-coated pits).

The AlexaFP-bound D71A mutant expressed on the bottom plasma membrane (which faces the coverslip) of CHO-K1 cells was observed by a home-built total internal reflection fluorescence (TIRF) microscope (Materials and methods, "Single FM imaging"). CHO cells were selected for this study because they allow the AlexaFP to readily enter the space between the bottom membrane and the surface of the coverslip, and thus it can rapidly equilibrate between the gap space and the bulk solution (Fig. 1, B and C; see the legend text for C and the first paragraph of Materials and methods). Based on the binding kinetics shown in Fig. 1 C, the receptor monomers and dimers were counted in the 6–8 min period after the addition of AlexaFP. The presence of such a gap also ensures the virtual lack of the effect of the coverslip on the dynamics and the monomer–dimer equilibrium of FPR in the bottom plasma membrane.

Establishing a single FM imaging method to determine the true dimer fraction in terms of the number of fluorescent spots

Defining colocalization of two molecules (optically unresolvable spots). A typical single-frame image of single AlexaFP molecules bound to D71A on the bottom plasma membrane, observed at 7 min after adding 1 or 6 nM AlexaFP, are shown in Fig. 2 A. Fluorescent spots in the image were identified by a homemade computer program, which takes the cross-correlation of the observed image with a reference 2D Gaussian function with a full width of 200 nm (Fujiwara et al., 2002). In addition to identifying the fluorescent spots, this method generates the local peaks in the correlation image (Fig. 2 B), and thus can determine whether an observed spot actually represents one unresolvable spot or two resolvable spots. In this manner, the number density of distinguishable spots (*NDDS*) was determined (we consider all of the spots detectable in the image, without any arbitrary omissions of the fluorescent spots).

Furthermore, the spatial resolutions of our microscope for single molecules of monomeric GFP (mGFP; an A206K mutant of GFP), AlexaFP (Alexa Fluor 594), and DY547 were all found to be ∼220 nm (219 ± 9.0 nm; Fig. 2, B and C; see Materials

binding at 6 nM had already achieved the equilibrium conditions at 6–8 min after its application (all of the observations were performed during this period). Furthermore, the ligand binding in the central region of the bottom membrane occurs as fast as that in the peripheral region (Fig. 1 B), which suggests that the ligand concentration within the space between the bottom membrane and the coverslip is rapidly equalized with that in the bulk space (indeed, one of the major reasons we selected CHO cells for this study is this fast entrance of the ligand in the space between the bottom membrane and the coverslip. For some cell types, the ligand reaches the central part of the bottom membrane quite slowly).

Figure 2. Counting the numbers of apparent monomer/dimer fluorescent spots of AlexaFP in a single-frame TIRF image. (A) A representative single-frame TIRF image of single AlexaFP molecules bound to D71A, observed at 7 min after the addition of 6 nM AlexaFP. Individual fluorescent spots were identified by taking the cross-correlation of the observed image with a reference image of a single FM spot. Yellow arrowheads and red arrows indicate the spots with monomeric and dimeric intensities (< and >18 AU in D), respectively. (B) This image cross-correlation method, in addition to identifying the fluorescent spots, finds the local peaks in the correlation image, determining whether an observed spot actually represents one unresolvable spot or two resolvable spots (bottom; spatial resolution). Here, a typical image of a single-molecule intensity spot is superimposed on itself but, at systematically varied shift distances between the two images (from 0 to 300 nm, every 10 nm along the x axis. Top, raw images; bottom, cross-correlation images, with red dots showing local peaks; typical examples using D71A-mGFP), and for each shift distance, the result of one or two peaks was registered in the cross-correlation images (bottom). (C) Determining the spatial resolution for single FM imaging. The process of B was repeated for 300 single FM spots with monomeric signal intensities (using images as in A). Then, for each shift distance, we obtained the percentage of fluorescent spots judged to be two space-resolved spots (standard error given as cell-to-cell variations, $n_{cell} = 6$), which was plotted as a function of the shift distance. The threshold shift distance was ~220 (219 ± 9.0) nm for mGFP. For the intensity-dependence of spatial resolution, see Materials and methods ("Determining the spatial resolution..."). (D) The distributions of the signal intensities of individual AlexaFP-D71A spots, fitted with the sum of the two Gaussian functions: one is consistent with single AlexaFP molecules with a peak value of ~12 AU (those bound to the coverslip, bottom); the other is a smaller, broader peak ~24 AU (9.7 and 23% of the spots in the medium containing 1 and 6 nM AlexaFP, respectively; top and middle).
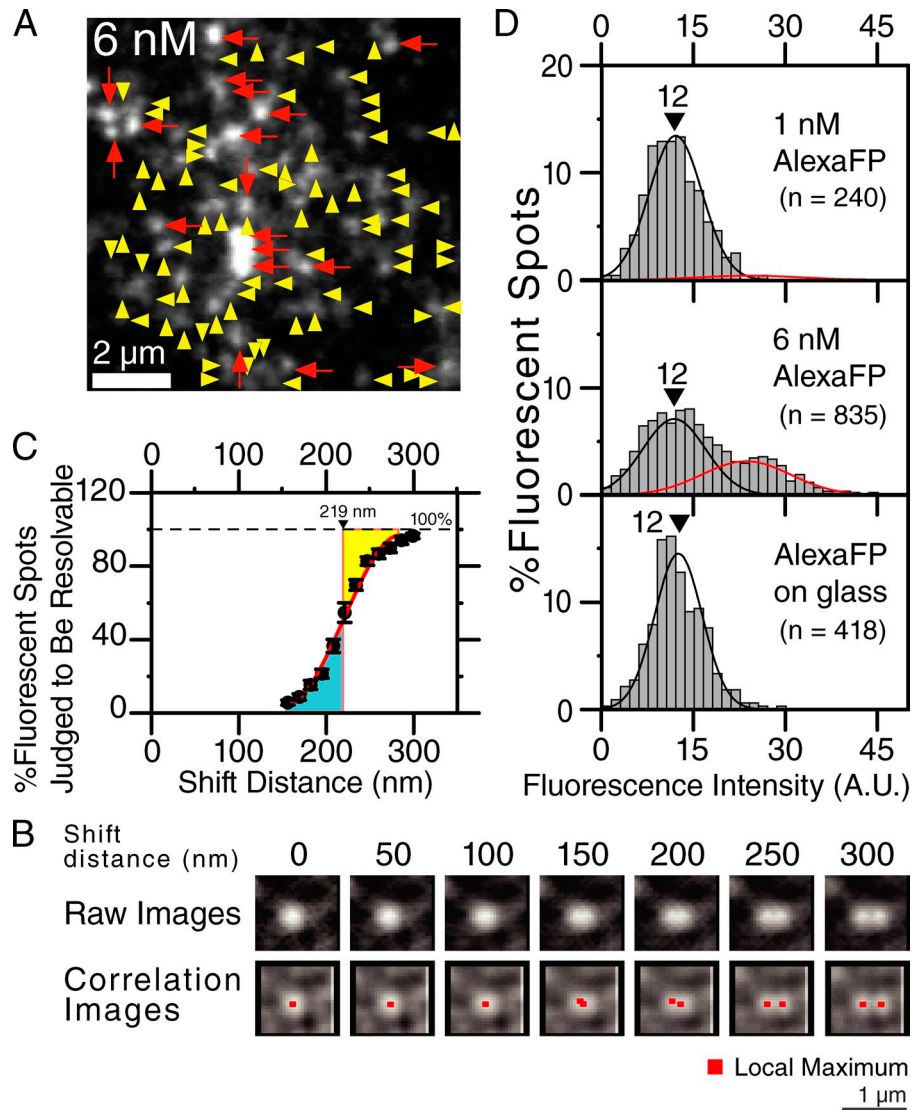
and methods, "Determining the spatial resolution for two spots...": Note that each value determined in this paper is given as the mean ± standard error, and, in the case of the fitting parameters, the fitting error at the 68.3% confidence limit is given), perhaps because the trade offs of the wavelength and the signal-to-noise ratio.

Determining the fraction of [true + apparent] dimer spots (P_{Dspot}^{T+A}) from the distribution of the signal intensity of each individual spot. After each individual spot in the image was identified, the signal intensities of all of the identified spots were determined, yielding the histograms shown in Fig. 2 D. These histograms were fitted by the sum of two Gaussian functions (Materials and methods, "Fitting the signal intensity histograms..."), and provided the spot fractions for monomer-like and dimer-like spots by comparison with the histogram for AlexaFP attached to coverslips, a control for monomers (monomer-like because these spots would contain dimers including one nonfluorescent receptor molecule; dimer-like because these

spots would contain incidentally overlapped monomers within 220 nm, which we call "apparent dimers" in this paper. Greater apparent oligomers are rare with the number-density range used here, see Fig. S1 A). The ratio of the number density of [true + apparent] dimer spots against *NDDS* is termed P_{Dspot}^{T+A}.

Evaluating the fraction of apparent dimer spots (two monomer spots incidentally located within the optical diffraction limit). Incidental approaches of two noninteracting receptors within the optical resolution limit will result in apparent dimers. As shown in Fig. S1, using computer simulation and the 220-nm spatial resolution, the fraction of incidentally overlapped spots (the fraction of apparent dimer spots, P_{Dspot}^{A}) can be evaluated as a function of the number density of all of the distinguishable fluorescent spots in the image, *NDDS*, and was found to be represented well by a second-order polynomial function,

$$P_{Dspot}^{A} = 0.075 \times NDDS + 0.00057 \times NDDS^2. \tag{1}$$

Experimental validation of Eq. 1, using monomer reference molecules, and evaluation of the fraction of true dimer spots. The validity of this simulated relationship was experimentally verified by using non-interacting molecules incorporated in the membrane (Fig. 3). As monomer reference molecules, we used an acyl carrier protein (ACP; covalently labeled with a single DY547-tag) conjugated to the transmembrane domain of low-density lipoprotein (LDL) receptor with a 12-aa cytoplasmic domain (without the internalization signal; ACP(DY547)-TM) and an unsaturated phospholipid, L-α-dioleoylphosphatidylethanolamine (DOPE), conjugated with Alexa Fluor 594 in its headgroup (Alexa594-DOPE). Typical single-molecule TIRF microscope images of these molecules expressed or incorporated in the bottom plasma membrane are shown in Fig. 3 A, and the signal-intensity histograms are shown in Fig. 3 B. These histograms were obtained at various $NDDS$, and P_{Dspot}^{T+A}, obtained by the fitting with the sum of two Gaussian functions, was plotted as a function of $NDDS$ (Fig. 3 C). These plots for ACP-TM and Alexa-DOPE agree reasonably well with the fitting function given by Eq. 1 (Fig. 3 C).

The fraction of true dimer spot density against $NDDS$ (P_{Dspot}^{T}) can be obtained by $P_{Dspot}^{T+A} - P_{Dspot}^{A}$, where P_{Dspot}^{A} is given by Eq. 1 (Fig. 3 D). Less than 4% of the distinguishable spots were found to represent true dimers, which is in acceptable agreement with the expected value of 0%.

In addition to this statistical estimate of P_{Dspot}^{T}, BiFC (Hu et al., 2002) was performed, which directly detected dimers at the molecular level, as described later (see Fig. 7).

Determining P_{Dspot}^{T+A} for FPR as a function of the expression level of D71A ($NDDS$)

P_{Dspot}^{T+A} for D71A was obtained as a function of $NDDS$, in the range of ∼0.3–2.5 copies/μm² (∼840–7,000 copies/cell for a spherical cell with a 15-μm radius; Fig. 4 A). Next, to obtain the 2D dissociation constant of dimers (2D-K_D), the x and y axes of Fig. 4 A must both be converted to values expressed in terms of the number density of molecules (ND_{mol}), rather than that of distinguishable spots ($NDDS$). To accomplish this conversion, the fraction of D71A that was actually labeled with AlexaFP (the labeling efficiency of D71A), f, was first determined.

Determining f

Determining the dissociation constant of AlexaFP from D71A. We first determined the dissociation constant of AlexaFP from D71A, because once it is known, the labeling efficiency f can be calculated from the AlexaFP concentration added to the medium (because the amount of AlexaFP molecules in the medium far exceeds that of D71A, even after AlexaFP binding, its concentration, L_c, is almost unchanged).

To determine the dissociation constant of AlexaFP from D71A and the number density of D71A expressed on the CHO cell surface, a 2D-3D Scatchard plot was generated (Materials and methods, Theory 2; Fig. S2). The plot was linear in the full range of AlexaFP concentrations used here. From the plot, the number density of the expressed D71A (ligand binding site) was found to be 1.6 ± 0.072 D71A copies/μm², and the ligand

dissociation constant was found to be 2.2 ± 0.17 nM. This value is in agreement with the previous result obtained by WT-FPR and the formyl peptide without a fluorescent tag, 1.8 ± 0.18 nM (a single dissociation constant; Dolmatch and Niedel, 1983).

Determining f of AlexaFP to D71A. In the experiments to obtain P_{Dspot}^{T+A} (Fig. 4 A) at various expression levels of D71A ($NDDS$), we always used an AlexaFP concentration of 6 nM. At this AlexaFP concentration, based on the equilibrium binding and the AlexaFP dissociation constant from D71A (2.2 nM), and using Eq. 14 in Materials and methods, Theory 2, $f = 0.73 ± 0.077$ was obtained.

Equations converting the number of spots to the number of molecules, using f

If $f = 1$, the numbers of monomer spots and dimer spots in the image are the same as those for the molecules. However, for more general and prevalent cases where f is smaller than 1, a theory taking $f < 1$ into account has been developed to evaluate the fraction of molecules existing as dimers from P_{Dspot}^{T} (equal to $P_{Dspot}^{T+A} - P_{Dspot}^{A}$, i.e., the ratio of true dimer spots vs. $NDDS$).

Let P_{Dmol} be the fraction of molecules in true dimers (against the total number of expressed molecules). P_{Dmol} can be approximated with <10% error as a function of P_{Dspot}^{T} and f, as

$$P_{Dmol} = \frac{2P_{Dspot}^{T}}{f \times (1 + P_{Dspot}^{T})},\qquad(2)$$

(Materials and methods, Theory 3).

Meanwhile, the x axis of Fig. 4 B, $NDDS$, can be converted to the number density of molecules expressed on the cell surface, ND_{mol}, using P_{Dspot}^{T+A} and f:

$$ND_{mol} = NDDS(1 + P_{DspotT+A}) / f,\qquad(3)$$

giving the x axis of Fig. 4 C (Materials and methods, Theory 1, Eq. 9).

Evaluating the 2D-K_D (2D dimer dissociation constant) for D71A

Let us define [M] and [D] as the number densities of true monomers and true dimers in the plasma membrane, respectively (Materials and methods, Theory 4). Then,

$$ND_{mol} = [M] + 2[D].\qquad(4)$$

The number density of molecules residing in dimers (y axis of Fig. 4 C) can be expressed as $2[D] = ND_{mol} \times P_{Dmol}$.

This is plotted as a function of ND_{mol} (determined by Eq. 3) in Fig. 4 C, and fitted with a function

$$2[D] = \frac{4 \times ND_{mol} + K_D - \sqrt{8 \times ND_{mol} \times K_D + K_D^2}}{4},\qquad(5)$$

where K_D (2D-K_D) is a fitting parameter (Theory 4). From the fitting, the best fit value for K_D was obtained as 3.6 ± 0.58 copies/μm².

At the physiological expression level of 6,000 FPR copies per cell (2.1 copies/μm², assuming a spherical cell with a
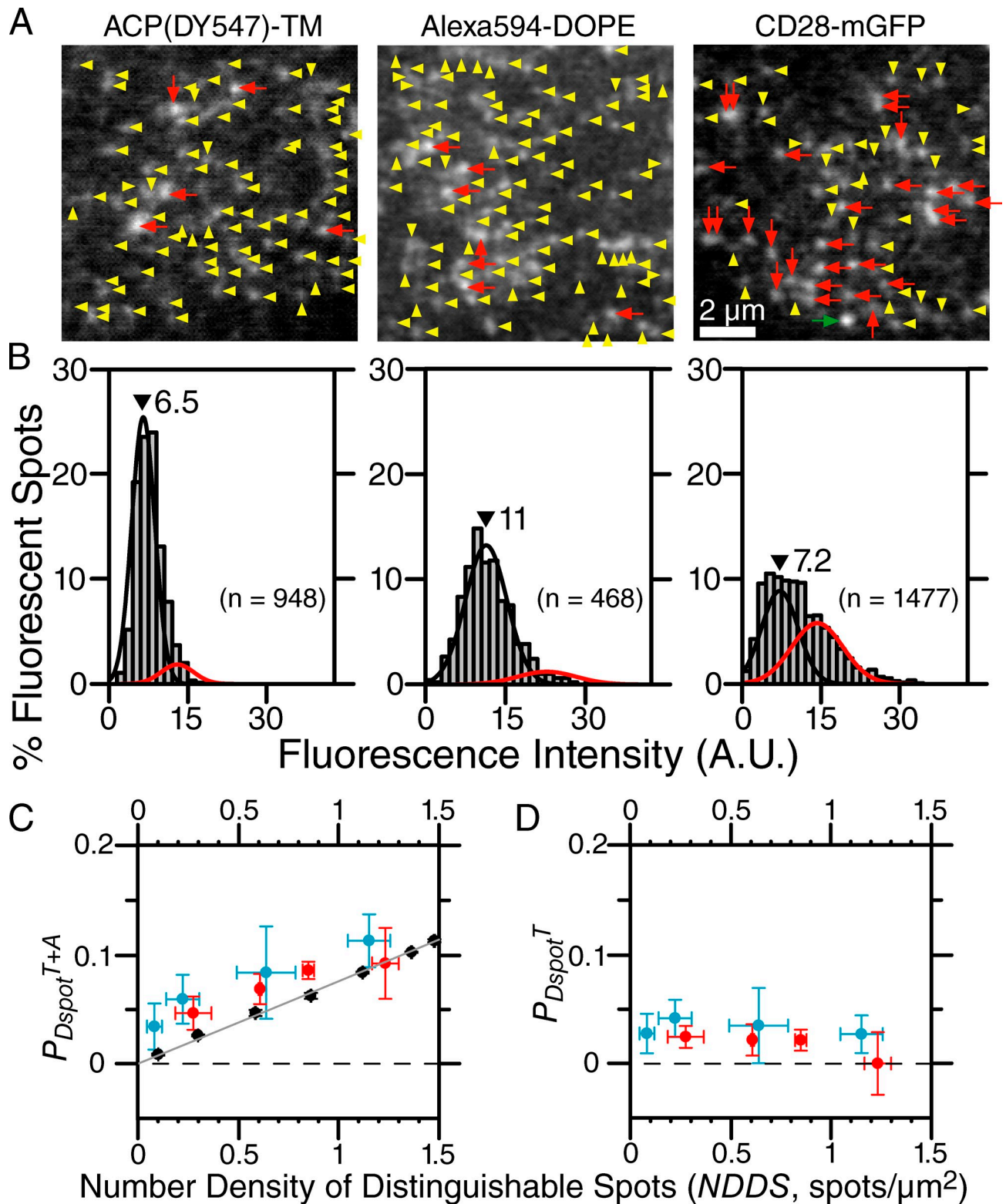
Figure 3. **Evaluating the fraction of incidentally overlapped spots as a function of the *NDDS*: experimental validation of Eq. 1.** (A) Representative single-molecule TIRF images of monomer reference molecules—ACP(DY547)-TM (left) and Alexa-DOPE (middle)—and a dimer reference molecule, CD28-mGFP (green arrow, tetramer-like spot). Yellow arrowheads and red arrows indicate the spots with monomeric and dimeric intensities, respectively. (B) Distributions of the signal intensities of individual spots, fitted with the sum of two Gaussian functions (apparent monomers and apparent dimers), giving P_{Dspot}^{T+A}. (C and D) P_{Dspot}^{T+A} (C) and P_{Dspot}^{T} (equal to $P_{Dspot}^{T+A} - P_{Dspot}^{A}$; D) plotted as a function of *NDDS*, for ACP(DY547)-TM (red) and Alexa-DOPE (blue), showing that these plots agree with the simulation result (black keys and the best fitting curve, $P_{Dspot}^{A} = 0.075 \times NDSS + 0.00057 \times NDDS^2$. For each data point, $1,550 < n_{spot} < 1,800$.
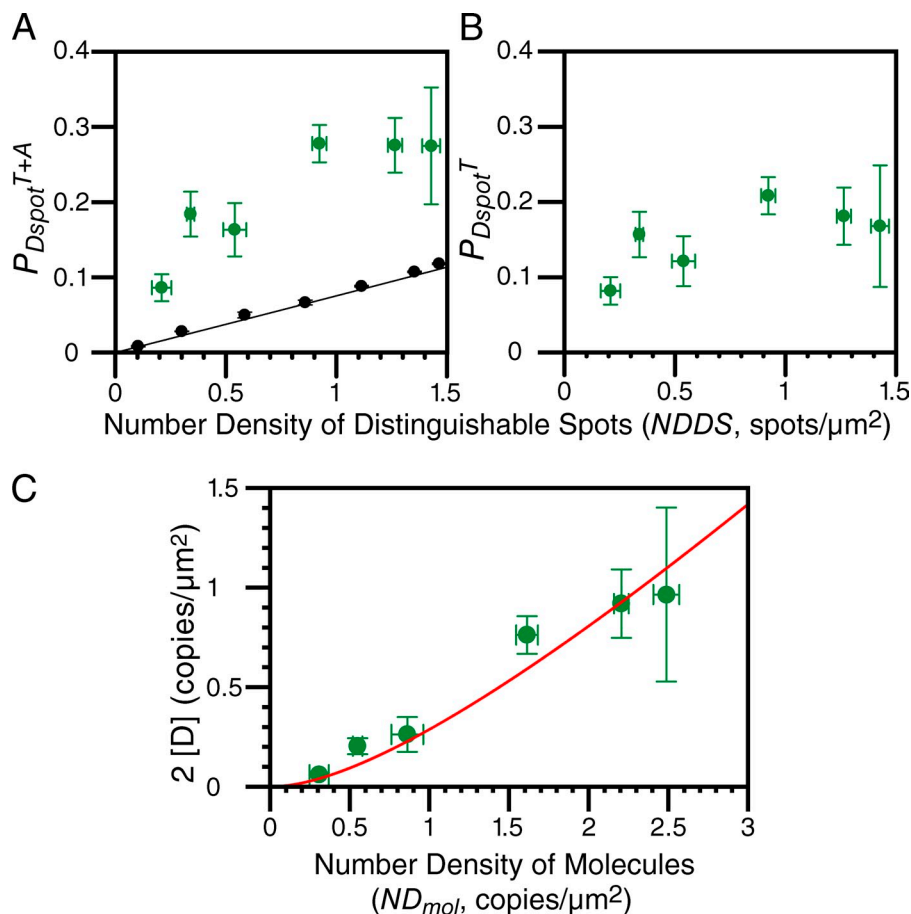
A

P_{Dspot}^{T+A}

0.4

0.3

0.2

0.1

0

0   0.5   1   1.5

Number Density of Distinguishable Spots ($NDDS$, spots/µm²)

B

P_{Dspot}^{T}

0.4

0.3

0.2

0.1

0

0   0.5   1   1.5

C

2 [D] (copies/µm²)

1.5

1

0.5

0

0   0.5   1   1.5   2   2.5   3

Number Density of Molecules
(ND_{mol}, copies/µm²)

Figure 4. **Determining f and 2D-K_D.** (A) P_{Dspot}^{T+A} plotted as a function of $NDDS$ (green; for each point, n_{cell} = 3, examining a total of ∼500 spots). Black keys and the line, P_{Dspot}^{A} (simulation). (B) P_{Dspot}^{T} (equal to $P_{Dspot}^{T+A} - P_{Dspot}^{A}$) plotted as a function of $NDDS$. (C) 2[D], the number density of molecules in true dimers, plotted as a function of the number density of expressed molecules (ND_{mol}), and fitted with Eq. 5 (red curve). The error bars are greater for samples at higher number densities (particularly the points around 2.3–2.5 copies/µm²) because of the crowding of the fluorescent spots in the image. To address this point, we fitted the data, assuming that the largest or the smallest values given by the error bar for the highest number density point are correct. The obtained 2D-K_D was 5.6 and 2.8 copies/µm², respectively, whereas the present estimate is 3.6 ± 0.58 copies/µm².

15-µm radius; Tennenberg et al., 1988), using Eq. 5 and 2D-K_D = 3.6 copies/µm², 0.43 dimers/µm² (0.86 dimer-incorporated molecules/µm²) and 1.24 monomers/µm² should exist; i.e., 41 and 59% of D71A molecules are in dimers and monomers, respectively, on average, at any time. This clarifies the controversies over the presence of GPCR dimers in the case of D71A. Note that, in this evaluation, incidental approaches of two molecules were subtracted, and therefore, the 2D-K_D obtained here is the value related only to true dimers. In addition, the formation of dimers at the molecular level (not colocalization at the optical resolution) was examined (see Fig. 7). Furthermore, the dimer–monomer equilibrium of WT-FPR and the effect of ligand binding to WT-FPR will be addressed later in this paper (compare Fig. 8 and related text): WT-FPR exhibited monomer–dimer equilibrium very similar to D71A examined here.

Application to the dimer reference molecule CD28

To examine whether this method can detect constitutive covalent dimers as dimers (∼100%), we applied it to CD28, which exists as a disulfide-linked dimer (Dorsch et al., 2009). We used CD28-mGFP, 95% of which we found exists as dimers by comparative nonreducing and reducing PAGE, followed by Western blotting (unpublished data).

From the results shown in Fig. 3 (A and B, right), it was concluded that 58% (P_{Dspot}^{T} = 0.58 ± 0.039) of the distinguishable spots represent true dimer spots (n_{cell} = 4, and 3,281 spots

were examined; see Materials and methods, "Application to the dimer reference molecule…" for details). Using Eq. 2 (with an estimate of f = 0.71, see "Application to the dimer reference molecule…" for details of evaluating f for CD28), P_{Dmol} (the fraction of molecules in dimers) was found to be 1.03, which indicates that ∼100% of the CD28-mGFP molecules exist as dimers, consistent with the SDS-PAGE result. This result validates the method developed here.

D71A dimers dissociate into monomers rapidly, with a lifetime of 91 ms

D71A dimers form and disintegrate continually. Single-molecule dynamics of D71A bound by AlexaFP were observed by TIRF microscopy at video rate. Fig. 5 displays a typical video sequence, showing that virtually all of the D71A molecules undergo diffusion and frequent colocalization and codiffusion with other D71A molecules. Each colocalization–codiffusion event often lasts longer than incidental approaches, followed by separation into monomers (Video 1). As described later, the results of the BiFC (Hu et al., 2002) revealed the occurrence of direct molecular interactions, i.e., dimer formation.

Dissociation rate constant for dimers (dimer lifetime). The duration of each colocalization event was measured at a time resolution of 4 ms, and the distribution of colocalization durations was obtained, as shown in the histograms in Fig. 6 A. The monomer reference molecule, ACP(DY547)-TM, exhibited incidental colocalization and thus

Figure 5. **D71A dimers continually form and disintegrate dynamically.** A typical video sequence (recorded and shown at a 33-ms resolution) showing three diffusing D71A(-AlexaFP) molecules and their trajectories (Video 1). Two molecules (green and red trajectories) first became colocalized in video frame 3 (67 ms), diffused together for 3 video frames (100 ms, see the trajectories; colocalization 1), and then separated. After diffusing as monomers for 133 ms, one of the two molecules (dark blue trajectory) became colocalized with a third molecule (pink trajectory) for 133 ms (colocalization 2), then separated.
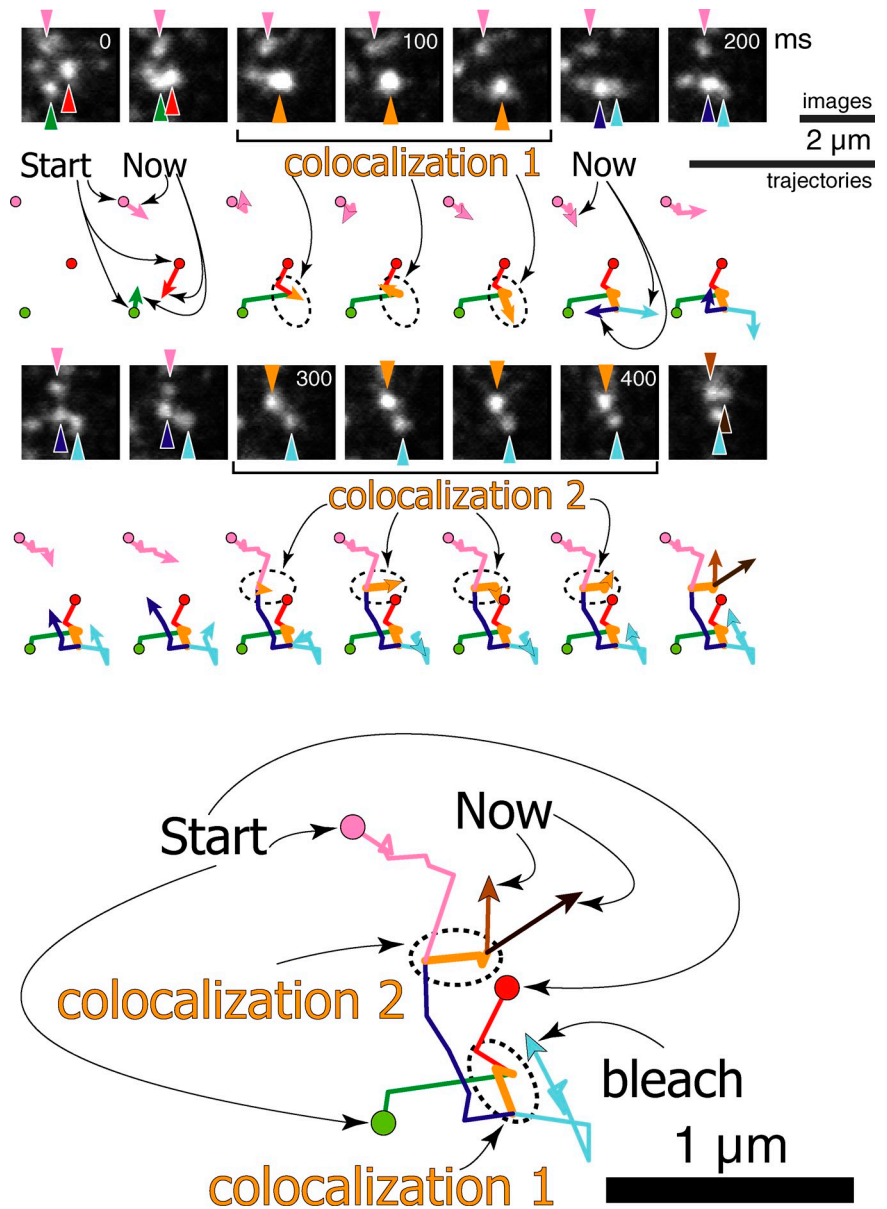
provided a duration histogram of the incidental colocalization events (Fig. 6 A, right). This histogram could be fitted well with a single exponential function with a decay time constant of 18 ± 0.61 ms, which would be a characteristic duration for the incidental approaches of two molecules, in the absence of molecular-level interactions.

The histogram for the durations of individual colocalization events for D71A (Fig. 6 A, left) observed at a 4-ms resolution indicates that the distribution could be fitted well with a single exponential function with a decay time of 63 ± 4.9 ms. However, because the D71A histogram should include the contributions of both specific and incidental colocalization events, it should be fitted with the sum of two exponential functions with two different decay time constants, one close to ∼18 ms for incidental approaches, and a longer one caused by specific molecular interactions. However, using the sum of two exponential functions was not successful (converging to a single

decay constant or one of the two falling into a meaningless value), probably because of the insufficient time resolution and/or low signal-to-noise ratios for detecting small fractions of apparent dimers. Therefore, we used the exponential decay constant obtained for D71A by a single exponential fitting as an effective colocalization duration.

The colocalization duration obtained from the histogram requires a correction for photobleaching of the fluorescent probe (Materials and methods, Theory 5). Defining the corrected dimer lifetime as $\tau_d{}^*$, the photobleaching lifetime for single FMs using the same images used for colocalization analysis as τ_b (Fig. 6 B; 295 ± 23 and 938 ± 66 ms for AlexaFP-D71A and ACP(DY547)-TM, respectively), and the lifetime directly determined from the colocalization histogram as τ_{app}, $\tau_d{}^*$ can be calculated by the following equation (Materials and methods, Theory 5, Eq. 22).

$$\tau_d{}^* = [\tau_{app}{}^{-1} - 2\tau_b{}^{-1}]^{-1}. \tag{6}$$

A: 4-ms Resol.

AlexaFP-D71A
$\tau_{app} = 63 \pm 4.9$ ms
($\tau_{off}^* = 110 \pm 16$ ms)
(n = 334)

ACP(DY547)-TM
$\tau_{app} = 18 \pm 0.61$ ms
($\tau_{off}^* = 19 \pm 0.66$ ms)
(n = 227)

% Colocalized Spots

Colocalized Duration (ms)

B: 4-ms Resol.

AlexaFP-D71A
$\tau_b = 295 \pm 23$ ms
(n = 220)

ACP(DY547)-TM
$\tau_b = 938 \pm 66$ ms
(n = 421)

%Fluorescent Spots

Lifetime (ms)

C: 33-ms Resol.

AlexaFP-D71A
$\tau_{app} = 96 \pm 6.3$ ms
($\tau_{off}^* = 116 \pm 9.6$ ms)
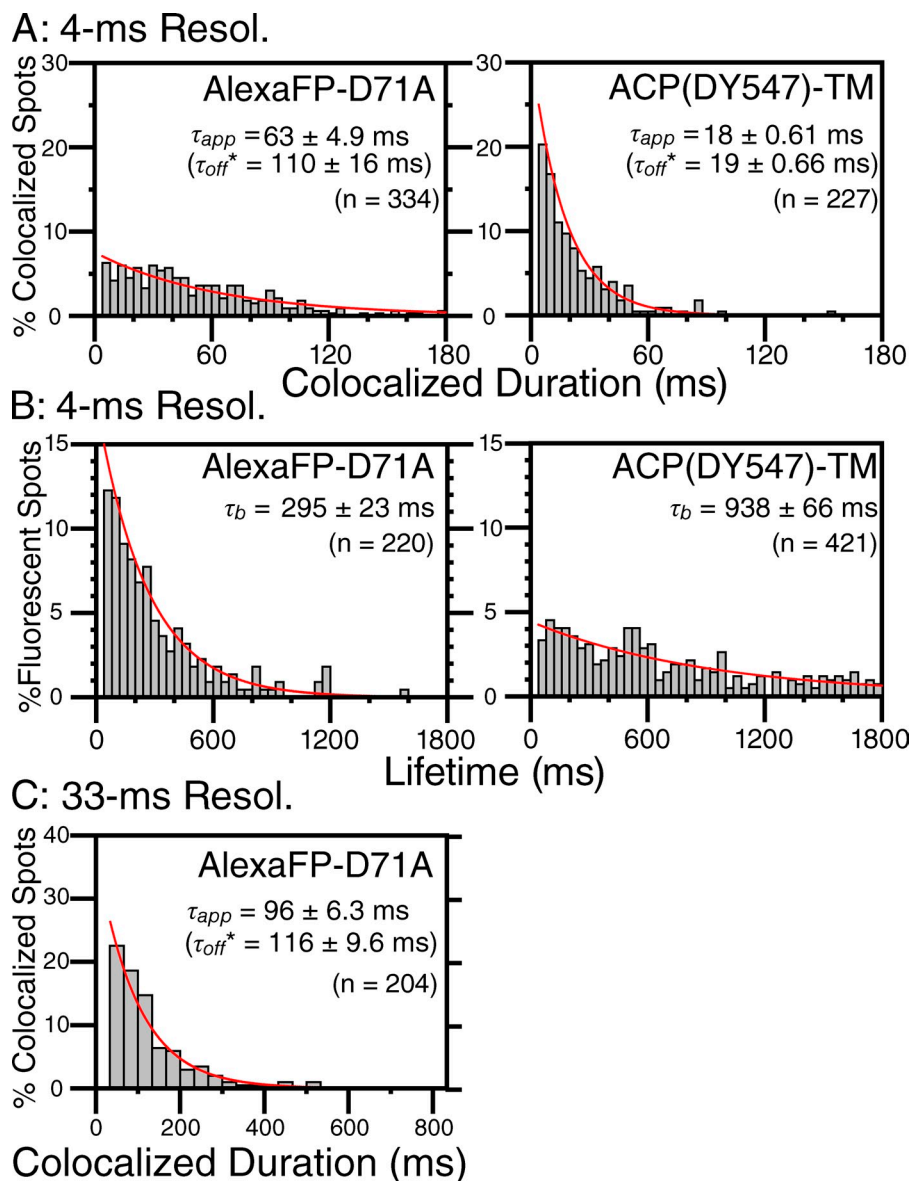(n = 204)

% Colocalized Spots

Colocalized Duration (ms)

Figure 6. Determining the dissociation rate constant for FPR dimer by observing single receptor molecules. (A) The distributions of the duration of each colocalization event for D71A (left) and a monomer reference molecule ACP(DY547)-TM (right), observed at a time resolution of 4 ms. (B) The distribution of photobleaching lifetime for each monomer spot. See the text for details. (C) The distribution of the duration of each colocalization event for D71A, observed at a 33-ms resolution.

In this equation, note that the notation τ_d^*, rather than τ_d used in Eq. 22 of Theory 5 (Materials and methods), is used to save the notation τ_d for the true dimer lifetime, described as follows. The τ_d^* values for D71A and ACP-TM were 110 ± 16 and 19 ± 0.66 ms, respectively, which suggests that the overall duration in a dimeric state (τ_d) would be 91 ± 16 ms (110–19 ms). Note that, because this duration might be the result of many dissociation-rebinding events, this number should be considered to be the collective lifetime when the dimerization did occur. The dimer dissociation rate constant can be obtained as $k_d = \tau_d^{-1} = 11.0 \pm 1.9$ s^{-1}. The on-rate (the rate constant for forming dimers) can be obtained as $k_a = k_d/K_D = 3.1 \pm 0.72$ [copies/μm^2]$^{-1}$s^{-1}. Namely, at the physiological expression level of 2.1 FPR copies/μm^2 (6,000 copies/cell; Tennenberg et al., 1988), monomers are continually converted into dimers every 150 ms and dimers are dissociated into monomers in 91 ms, whereas on average (as described right after Eq. 5), 41% of D71A exists as transient dimers at any moment (2,500 molecules

in dimers = 1,250 dimers, and 3,500 molecules in monomers). Therefore, one should note that not only do dimers "fall apart" rapidly, but monomers also convert to dimers very quickly.

Meanwhile, τ_d^* was also estimated as 116 ± 9.6 ms at a time resolution of 33 ms (the overall observation duration for each dimer was extended by a factor of ~8; Fig. 6 C), which agrees well with 110 ± 16 ms obtained at a 4-ms resolution, showing that long-lived dimers would be rare.

FPR dimers directly detected by YFP BiFC

In the experiments for detecting the colocalization of two single molecules, although incidental approaches are always considered and subtracted, the direct observation of molecular-level interactions is desirable. Our attempt to detect FRET did not work, perhaps because the location of the attached probe (the C terminus of FPR) was not favorable. Therefore, we used YFP BiFC to detect FPR dimers at the molecular level. In BiFC, two potentially interacting proteins are fused to N- and C-terminal

Figure 7. **BiFC detection of D71A dimers, showing the occurrence of interactions at the molecular level between two D71A molecules.** (A) A typical image of BiFC-D71A (D71A-YN and D71A-YC complex) spots, obtained by single-molecule TIRF imaging (a frame time of 33 ms) and identified by the image cross-correlation method (indicated by arrowheads). (B) The number densities of the observed BiFC fluorescence spots for BiFC-D71A (green) and BiFC-ACP-TM (red) were plotted as a function of the number densities of expressed molecules (ND_{mol}). The lines are to help the eye. (C) The lifetime of each individual fluorescent spot was observed, and their distributions are shown for YFP, BiFC-D71A, and BiFC-ACP-TM. See the text for details.
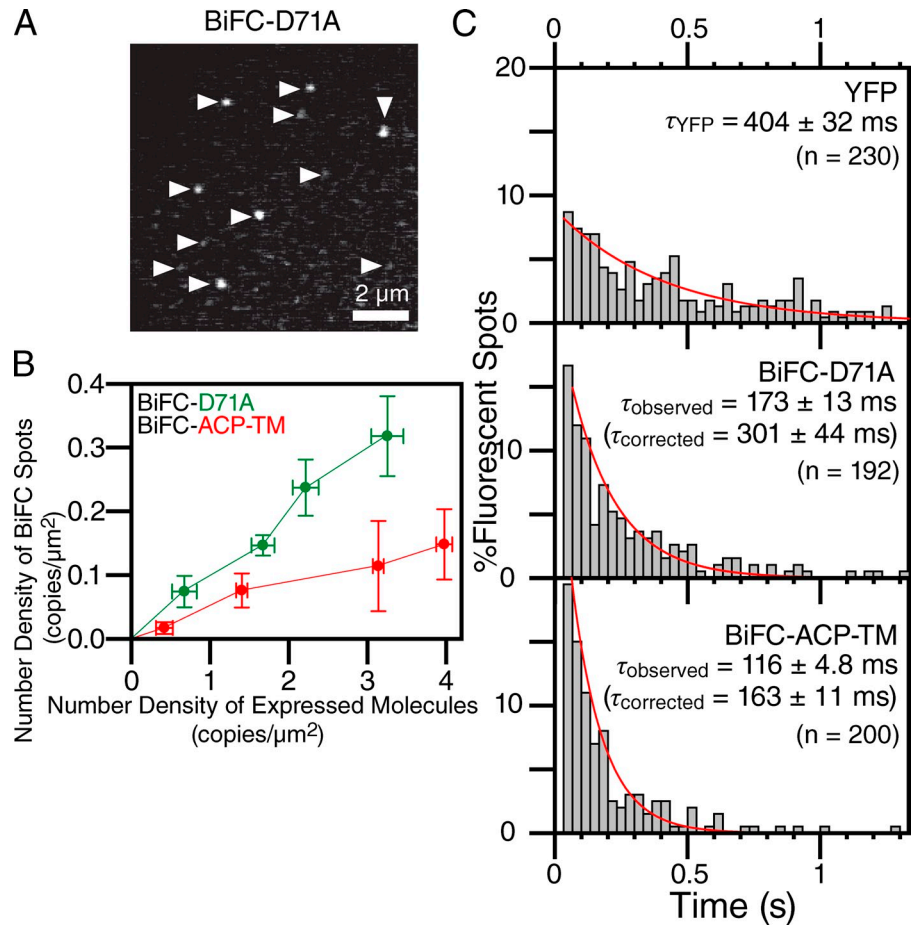
half-molecules of YFP, respectively. If these fusion proteins interact, YFP may be reconstituted (Hu et al., 2002; Miyawaki and Karasawa, 2007). Thus, if BiFC occurs, it would lend strong support for D71A dimer formation.

Here, the N- and C-terminal half-fragments of YFP were conjugated to the C terminus of D71A (D71A-YN and D71A-YC, respectively), and were expressed in the plasma membrane of CHO-K1 cells (the same cell line throughout this study). BiFC of the D71A-YN/-YC pairs (BiFC-D71A dimers) could be detected by single-molecule imaging as fluorescent spots (Fig. 7 A). When only either YN- or YC-linked D71A molecules were expressed, practically no fluorescent spots were observed, showing that the observed fluorescent spots are caused by BiFC.

To quantitatively examine BiFC, BiFC of D71A and that of a monomer reference molecule, ACP-TM (using ACP-TM-YN and ACP-TM-YC), were compared as a function of their expression levels (Fig. 7 B; the expression levels were determined by the addition of AlexaFP and DY547-ACP ligand, respectively). As shown in Fig. 3, under the expression conditions of ACP(DY547)-TM used in the present study, it behaved almost exactly like Alexa Fluor 594–DOPE (a typical nonraft phospholipid), which indicates that ACP(DY547)-TM is a good monomer reference molecule. The number density of expressed molecules (ND_{mol}) was determined as described previously, using Eq. 3 (f = 0.73 [determined here as described] and 0.95 [Meyer et al., 2006], respectively). With increases in the number

densities of expressed molecules, the number densities of BiFC spots were increased for both molecules, but that of the BiFC-D71A-dimer spots was always greater than that of the BiFC-ACP-TM dimer spots by factors of 2–3 at the expression levels examined here (Fig. 7 B). This result indicates that although the molecular interactions of the probes, YN and YC, might contribute to inducing the BiFC fluorescent spots, the molecular interactions between D71A molecules contribute more to forming D71A-YN/-YC dimers.

As described in the previous paragraph, because an f of ∼1 (0.95) is realized with ACP (Meyer et al., 2006), one might wonder why we did not use ACP-FPR for determining the dimer fraction (as described, if f = 1, converting spot numbers to molecular numbers is much simpler. In addition, if ACP-FPR could have been used, the use of fluorescent ligand and the mutant D71A could have been avoided). However, this could not be done for the following reason. For ACP to work, the ACP moiety must be placed on the extracellular surface because the binding of the fluorescent ACP ligand to the ACP moiety requires an externally added enzyme, phosphopantetheine transferase. However, all of our attempts to express ACP-FPR in the plasma membrane failed.

The lifetime distributions of BiFC dimers were examined by measuring the fluorescent duration of each individual BiFC spot (histograms shown in Fig. 7 C, middle and bottom). These results clearly indicate that the BiFC dimers, formed

by inter-D71A as well as YN–YC interactions, are in dynamic equilibrium between dimers and monomers (YFP formed by YN and YC is not stable, dissociating into YN and YC in ~160 ms; Fig. 7 C, bottom), which is consistent with the reversible YN/YC binding described by Guo et al. (2005) and Anderie and Schmid (2007). These histograms could be fitted with single exponential functions (lifetime = $\tau_{observed}$), and after the correction for the photobleaching lifetime of YFP (Fig. 7 C, top; YFP's photobleaching lifetime = τ_{YFP} = 404 ± 32 ms), the corrected lifetimes for BiFC D71A-YN/YC and ACP-TM-YN/YC dimers ($\tau_{corrected}$) were calculated using the equation $\tau_{corrected}^{-1} = \tau_{observed}^{-1} - \tau_{YFP}^{-1}$, as 301 ± 44 and 163 ± 11 ms, respectively.

These values are substantially longer than the lifetimes of D71A and ACP-TM dimers (110 and 19 ms, respectively; Fig. 6 A), which indicates that YN/YC binding strongly contributes to prolonging the lifetimes of the BiFC dimers. Nevertheless, the difference in lifetimes between BiFC-D71A and BiFC-ACP-TM dimers is clear, which strongly indicates that D71A forms dimers.

Comparison between D71A and WT-FPR: ligand-binding effect

Next, we examined whether the WT forms transient dimers similar to those of D71A by comparing the behavior of D71A-mGFP with that of WT-mGFP, both before and after ligation (Fig. 8 A). A typical TIRF single-frame image of single WT-mGFP molecules expressed on the bottom cell membrane of a live CHO cell (no ligand) is shown in Fig. 8 B.

At similar mean expression levels of 0.75 ± 0.11 spots/μm^2 for both WT-mGFP and D71A-mGFP, the distributions of the fluorescence signal intensities of individual spots were determined (Fig. 8 C, third and fifth panels, respectively; also see the mGFP monomer controls in the top and second panels). Based on these data, $P_{Dspot}{}^T$ was estimated as was done for AlexaFP-D71A, and was 13 ± 3.2% for D71A-mGFP (five cells, 1,372 distinguishable spots examined) and 13 ± 3.4% for WT-mGFP (11 cells, 6,264 distinguishable spots examined), clearly showing that the P_{Dspot} values for D71A-mGFP and WT-mGFP were similar to each other.

Furthermore, $P_{Dspot}{}^{T+A}$ (and thus $P_{Dspot}{}^T$) of D71A-mGFP and that of WT-mGFP (the spots with intensities >25 AU, representing 4.2% of the spots, were excluded as they most likely represented molecules concentrated in clathrin-coated pits) did not significantly change after ligand application (100 nM formyl peptide, sufficient to nearly saturate the receptor within 1 min; Fig. 8 C, sixth and fourth panels, respectively). It follows then that the 2D-K_D for WT-mGFP (and thus WT) is similar to that of the AlexaFP-bound D71A, and that it does not change after liganding.

Discussion

In this paper, we have fully characterized the dynamic equilibrium between dimers and monomers for the first time for any membrane molecule by determining three critical parameters—2D-K_D, k_d, and k_a—using a GPCR as an exemplary paradigm (Fig. 9). We developed a single FM imaging method, considering the nonunity f (the actual fluorescent fraction of the receptor). Previously, f had almost always been assumed to be 1 in evaluating expression levels (often with GFPs), generating inaccurate estimates of the true receptor density and the number of dimers. Sugiyama et al. (2005) and Ulbrich and Isacoff (2007) successfully determined f for GFP (f = 0.67 − 0.80 and 0.795, respectively), but their methods are applicable only to protein aggregates and oligomers that are stable and basically uniform in size. Namely, they could not be used to determine f in the presence of coexisting and dynamically interchanging monomers and dimers.

Now that the manner in which f could be incorporated in the protocol for evaluating the dynamic monomer–dimer equilibrium has been established, and other steps, which require due caution for proper execution but are in principle trivial, have been described here, the super-quantification of dynamic monomer–dimer equilibrium is possible for virtually any molecular species located in or on the plasma membrane that can be quantitatively labeled with a fluorescent probe, in live cells and under physiological conditions. The overall flow for the determination method is summarized in Materials and methods ("The overall flow for the complete determination…").

The occurrence of molecule-level interactions of FPR was confirmed by the BiFC method. With the three critical parameters obtained here, the FPR dynamic equilibrium between monomers and dimers at 37°C is fully described. At a physiological expression level of 2.1 FPR copies/μm^2 (6,000 copies/cell; Tennenberg et al., 1988), monomers are continually converted into dimers every 150 ms, dimers are dissociated into monomers in 91 ms, and on average, 41% of D71A exists as transient dimers at any moment (2,500 molecules in dimers = 1,250 dimers and 3,500 molecules in monomers). Such a vivid description was previously possible.

Note that the 91-ms dimer lifetime found here is much longer than the durations of bimolecular collisions occurring on the molecular scale in the membrane (1–100-ns scales; East et al., 1985; Subczynski et al., 1990), which suggests that such a 100-ms level GPCR association, more than a millionfold longer than the durations of simple bimolecular collisions in the membrane, could have important biological significance. The presence of transient GPCR dimers observed here is consistent with the FRAP observations made by Dorsch et al. (2009), and would explain the reason why they were missed previously (Gripentrog et al., 2003). The exact values found here are those averaged over the entire cell surface, as these values would be locally influenced by any heterogeneity in the distribution of FPR molecules in the plasma membrane (Fig. 2 A).

The physiological expression levels of BAR is 41–260 copies/μm^2 (Mercier et al., 2002) or 16–160 copies/μm^2 (James et al., 2006), and that of neurokinin-1 receptor (NK1R) is 50–100 copies/μm^2 (Meyer et al., 2006). These values are ~10–100-fold greater than that of FPR (2.1 FPR copies/μm^2). If the 2D-K_D for BAR or NK1R is comparable to that for FPR, then under their physiological expression conditions, which are ~10-100-fold higher than those for FPR, 75–90% (respectively) of BAR or NK1R would exist as dimers. This result is consistent with previous observations (Angers et al., 2000; Mercier et al., 2002;

Figure 8. **Single FM imaging of WT-mGFP and D71A-mGFP before and after the addition of the nonfluorescent ligand FP, for comparing liganded D71A with unliganded WT.** (A) A schematic drawing of WT-mGFP and D71A-mGFP. The ligand was not labeled in the experiments shown here. (B) A representative TIRF single-molecule image of WT-mGFP expressed on the bottom cell membrane of a live CHO cell (no ligand). Yellow arrowheads and red arrows indicate spots with intensities < and >18 AU, respectively (see C and the legend for Fig. 2 A). (C) The distributions of the fluorescence signal intensities of individual spots. They were fitted with the sum of two Gaussian functions: the best-fit functions for the top two boxes became single Gaussian functions, whereas those for the bottom four boxes were the sum of two Gaussian functions. First and second panels, Monomer-reference molecules of mGFP. First box, mGFP expressed in and purified from *E. coli*, and nonspecifically adsorbed on coverslips. Second panel, mGFP-Gβ1, a subunit of trimeric G-protein, expressed in the plasma membrane of CHO cells. Note that the distributions of these two specimens are very similar to each other. Third and fourth panels, WT-mGFP expressed on the cell surface before and after the addition of 100 nM FP ligand (nonlabeled), respectively. The spots with signal intensities >40 AU probably represent molecules assembled in the internalization apparatuses. Fifth and sixth panels, D71A-mGFP expressed on the cell surface before and after the addition of 100 nM FP ligand, respectively.
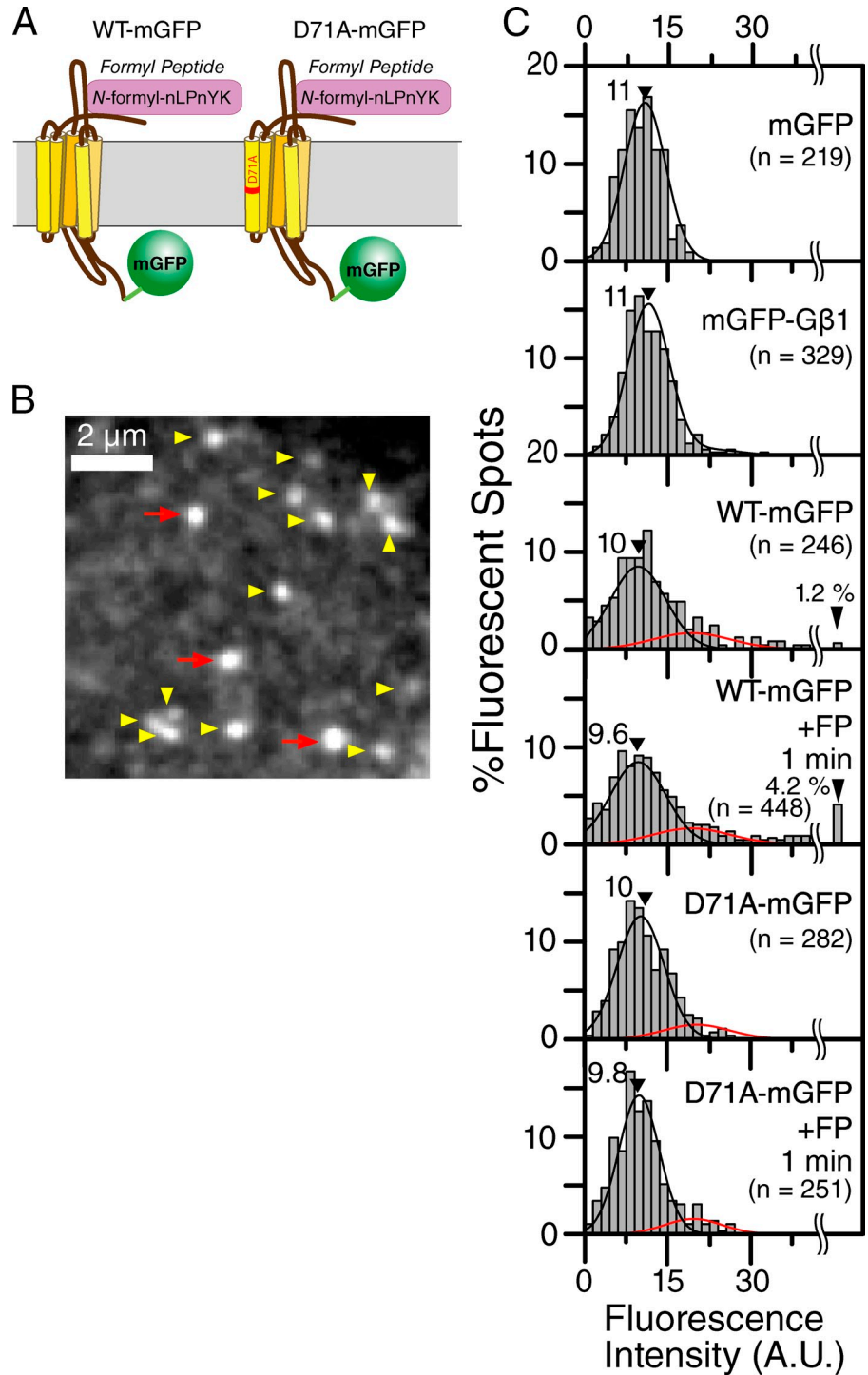
James et al., 2006; Meyer et al., 2006), and with the in vitro data for neurotensin receptor 1 reconstituted membrane described by Harding et al. (2009). However, one should realize that, even under the conditions where dimers are predominant, they are likely to fall apart with lifetimes of 91 ms or so.

Ligation of FPR does not appreciably change the dimer–monomer equilibrium, which is consistent with the neurokinin-1 receptor data (Meyer et al., 2006). However, like many other receptors, transient dimers of FPR might be important for accelerating signal transduction (Chung et al., 2010), raising or lowering the average binding/dissociating kinetics of trimeric G proteins and GPCR kinases (Hebert et al., 1996; Wenzel-Seifert and Seifert, 2003; Bulenger et al., 2005) and thereby regulating the interactions with the downstream molecules (Damian et al., 2006). Furthermore, FPR transient dimers might be important as a drug discovery target, because drugs that can divalently bind to FPR dimers would have much higher affinities to FPR (Miller et al., 2009).

In addition to signaling, transient dimerization might be involved in regulating receptor trafficking. For example, GPCR
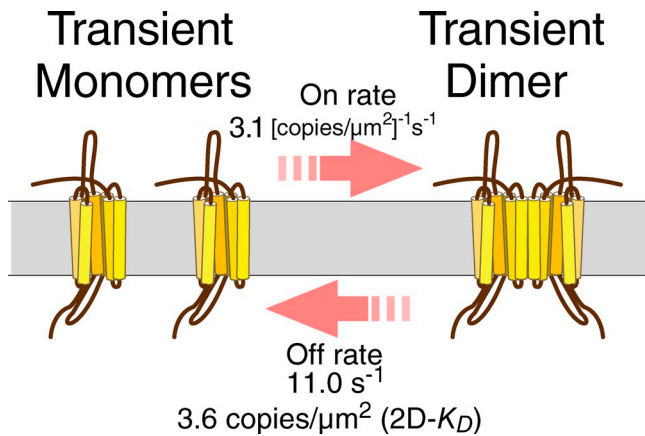
Transient Monomers

Transient Dimer

On rate
3.1 [copies/μm^2]$^{-1}$s^{-1}

Off rate
11.0 s^{-1}

3.6 copies/μm^2 (2D-K_D)

Figure 9. Dynamic equilibrium of FPR between monomers and dimers with three kinetic parameters, on rate, off rate, and 2D-K_D. In the case of FPR, the ligand binding did not affect the dynamic monomer–dimer equilibrium.

homodimerization might be required for cell-surface targeting (BAR; Salahpour et al., 2004) or endocytosis (yeast α factor receptor [Overton and Blumer, 2000], BAR [Cao et al., 2005]). Under physiological expression conditions, although the dimer lifetimes might be limited ($\sim$100 ms), monomer lifetimes could be even shorter. Therefore, transient dimers might enhance average probabilities of the GPCRs getting on board the trafficking machineries.

Collectively, the present results indicate a general possibility that cellular signaling and trafficking might function and be regulated stochastically. There might only be transient, rather than stable, dimers and monomers of receptors, but the function of the receptor could still be regulated by the rapid conversions between dimers and monomers, and the average dimer/monomer ratios. Such dynamic regulation could provide means to regulate receptor functions much faster and locally by regulating local receptor concentrations by endocytosis, recycling, and membrane skeleton–controlled hop diffusion of receptor molecules (Kusumi et al., 2005; Suzuki et al., 2005; Chung et al., 2010).

Presently, most of our knowledge on the signal transduction in the plasma membrane has remained at qualitative levels. For the fundamental, mechanistic understanding, the next critical step is quantitative modeling based on exact quantifications, such as the three key parameters for monomer–dimer equilibrium and the number densities of receptor molecules, as determined in this study.

Materials and methods

General: five important experimental points used throughout this research
(1) All of the observations were made at 37°C. (2) FPR (D71A and WT) molecules expressed in the bottom plasma membrane of living CHO cells, which do not express detectable levels of endogenous FPR, were observed. As described in the main text, AlexaFP readily equilibrates between the bulk solution and the space between the bottom membrane and the coverslip. (3) The bottom cell membrane of CHO cells is considered to be rather flat in the observed area of $\sim$20 μm in diameter, in the central region of the illuminated area, based on the following observations. (3 a) In Fig. 2 D, the fluorescence signal intensity histogram for AlexaFP bound to the cell surface (D71A) at low concentrations (top) is very similar to that bound to the coverslip (bottom). (3 b) In Fig. 8 A, the fluorescence

signal intensity histogram for mGFP conjugated to Gβ1, a monomer reference molecule located on the plasma membrane (second panel), is very similar to mGFP bound to the coverslip (top). (3 c) Rapid-freeze, deep-etch electron microscopy of the bottom membrane (prepared by "unroofing" the top membrane) revealed a flat membrane for each view field of >20 μm in diameter (Morone et al., 2008). (4) Each value determined in this paper is given as the mean ± standard error, and, in the case of the fitting parameters, the fitting error at the 68.3% confidence limit is given. (5) In the present research, the expression levels we used were 0.3–2.5 copies/μm^2. Such low levels were required for the following three reasons: (1) for estimating K_d, the expression levels must be comparable to K_d, (2) the physiological expression level of FPR was reported to be 2.1 FPR copies/μm^2 (6,000 copies/cell; Tennenberg et al., 1988), and (3) to carry out single-molecule tracking, we have to limit the expression level under 2.6 copies/μm^2 (for avoiding too much overlapping of the fluorescent spots in the image).

Plasmid construction
The cDNA encoding full-length, WT-FPR (ppSSFV.neo; Prossnitz et al., 1993), with the linker sequence 5′-FPR-GCAGGTGCTAACGGTGCG-GCCGCT-3′ added to the 3′ end, was cloned into the pcDNA3+ vector (Invitrogen). An mGFP mutant (A206K = mGFP; Zacharias et al., 2002) cDNA, with the linker sequence 5′-GCGGCCGCT-3′ added to the 5′ end, was then placed in this vector, yielding the FPR-mGFP expression vector. The vector for the D71A mutant fused to mGFP was produced in a similar manner. For the generation of the ACP-TM cDNA, the signal sequence from rabbit LPH (5′-ATGGAGCTCTTTTGGAGTATAGTCTTTACT-GTCCTCCTGAGTTTCTCCTGCCGGGGGTCAGACTGGGAATCTCTG-3′) was attached to the N terminus of ACP, which was further conjugated to the transmembrane domain of 24 aa plus 10 aa of the cytoplasmic domain of LDL receptor (768–801 aa) at the C terminus of ACP.

The expression vector encoding CD28-mGFP was generated by a modification of CD28-sapphireGFP, a gift from S.J. Davis and J.R. James (University of Oxford, Oxford, England, UK; James et al., 2006), by replacing the sapphireGFP sequence with the mGFP sequence. CD28-mGFP was transiently expressed in CHO cells.

For the BiFC experiments for FPR and ACP-TM, the N-terminal YFP fragment (amino acids 1–155) and the C-terminal YFP fragment (amino acids 156–242), used by Briddon and Hill (2007), were produced from the pEYFP-C1 expression vector (Takara Bio Inc.) by using PCR with a linker (5′-CTCGATCTGATCGAAGGTCGTGGTATCCCTCGTAACTCTCGTGTTGAT-GCGGGA-3′), and were conjugated at the C terminus of FPR or ACP-TM.

For the experiments to determine f for mGFP using ACP-TM-mGFP, mGFP with a linker (5′-GAGGATCTGTACTTTCAGAGC-3′) was conjugated at the C terminus of the ACP-TM molecule.

Cell culture and cDNA transfection
CHO-K1 cells were maintained in Ham's F12 medium (Sigma-Aldrich), supplemented with 10% fetal bovine serum (Sigma-Aldrich), 100 units/ml penicillin, and 0.1 mg/ml streptomycin, and were transfected with various cDNAs using LipofectAMINE Plus (Invitrogen), according to the manufacturer's recommendations. For fluorescence microscopy, cells were plated on 12-mm glass-bottom dishes (Iwaki) and were used in 48–60 h. The culture medium was replaced with HBSS buffered with 2 mM of Pipes, pH 7.4, before observation.

Preparation of the formyl peptide with a single fluorescent probe
An *N*-formylated hexa-amino-acid peptide, *N*-formyl-Nle-Leu-Phe-Nle-Tyr-Lys (Nle, norleucine; Sigma-Aldrich), was tagged with Alexa Fluor 594 at the ε-amine of the single lysine group located at the C terminus (the α-amine is formylated, and could not be conjugated) by incubating 0.41 mM peptide and 9.33 mM Alexa Fluor 594 succinimidyl ester in 0.1 ml dimethyl formamide (dried with CaH$_2$, final concentrations) at 25°C for 4 h (dye/peptide ratio = $\sim$23), and was purified by silica gel thin-layer chromatography (Silicagel 70 Plate; Wako; developed by chloroform/methanol/acetic acid/water 60:40:2:2 by vol). The spot at a relative mobility of R$_F$ = 0.3 was scraped off and extracted with dimethyl formamide. Almost all of the peptide molecules were found to be conjugated with the fluorescent dye, and the parent peptide spot was barely visible. In addition, the absence of the parent peptide and the free dye in the eluted material was confirmed by reverse-phase HPLC (Hitachi; with an YMC ODS-AQ column, 150 × 6.0 mm) using a gradient from 1 to 80% acetonitrile with 0.1% HCl (vol/vol). This result indicated that each peptide molecule was conjugated with at least one dye molecule.

The actual dye/peptide ratio was determined by measuring the amounts of the peptide by amino acid analysis, and the amounts of the

attached Alexa Fluor 594 dissolved in water by optical absorption spectroscopy, using an extinction coefficient of 92,000 $M^{-1}cm^{-1}$ at 590 nm in water (pH 7.0). The dye/peptide ratio of the final product of AlexaFP was 0.96 ± 0.05, with an AlexaFP yield of ~30%. The AlexaFP was stored in dimethylformamide (3 µM).

ACP-TM expression and Alexa Fluor 594–DOPE incorporation in the plasma membrane of live CHO cells

A monomer reference molecule, ACP-TM, was transiently expressed in CHO cells, and was labeled with DY547-conjugated coenzyme A, an ACP synthase substrate, according to the manufacturer's instructions (Covalys Biosciences AG; George et al., 2004).

Another monomer reference molecule, Alexa Fluor 594–DOPE, was custom-ordered from Invitrogen and was incorporated in the plasma membrane of CHO cells, as described previously (Umemura et al., 2008). In brief, 4 µM of Alexa Fluor 594–DOPE in methanol was mixed with HBSS buffered with 2 mM of Pipes, pH 7.4, by vigorous vortexing (40 nM final concentration), and this solution was added to the cells cultured on a 12-mm glass-bottom dish at 37°C.

Single FM imaging

Fluorescently labeled molecules located on the bottom cell membrane (which faces the coverslip) were observed at 37°C with a home-built objective lens–type TIRF microscope (Tokunaga et al., 1997), constructed on an inverted microscope (IX-70; Olympus), as described previously (Iino et al., 2001; Nakada et al., 2003; Murakoshi et al., 2004; Koyama-Honda et al., 2005). The bottom membrane was locally illuminated with an evanescent field (~15 µm in diameter; 100×, 1.4 NA objective lens, 400× total magnification). The incident laser power was set such that its power was 1 mW after passing through the center of the objective lens. A two-stage microchannel plate intensifier (C8600-03; Hamamatsu Photonics), lens-coupled to an electron bombardment charge-coupled device camera operated at video rate (C7190-23; Hamamatsu Photonics) was used, and the obtained images were recorded on a digital videotape (PDV-184ME; Sony).

Each individual fluorescent spot was identified by using a home-made computer program as described previously (Fujiwara et al., 2002). The fluorescence signal intensities of all of the distinguishable fluorescent spots, determined as shown in Fig. 2 and described in its related main text, were measured in 520 × 520-nm areas (8-bit images in 10 × 10 pixels) containing the single spot, and the background intensity of an adjacent 520 × 520 nm area was always subtracted (Iino et al., 2001; Murakoshi et al., 2004; Koyama-Honda et al., 2005). To avoid the photobleaching effect on the observed image as much as possible, these intensity measurements were performed for images taken within 0.3 s after opening the excitation beam shutter.

We do not believe that the existence of FPR in the cytoplasm, if any, affects our measurements because of the following reasons. (a) When we observed WT- and D71A-mGFP (the probe attached at the C terminus) using an oblique-angle illumination mode of the TIRF illumination (with various angles) to see the cytoplasm and the top surface of the plasma membrane, we detected virtually no signals from the cytoplasm. (b) Furthermore, we found virtually no signals from the endosome-like vesicular structures in the cytoplasm after incubating the cells expressing WT-mGFP with the nonlabeled FP ligand for 1 min (conditions for results shown in Fig. 8). (c) When the same experiments were performed with D71A (D71A-mGFP), virtually no internalization was detected for 1–20 min after the addition of AlexaFP (nonlabeled FP). Please note that, in the experiments using the fluorescent AlexaFP ligand, we always used D71A, and we detected no signs of receptor assembly in the plasma membrane or internalization. Based on these observations, we conclude that our single-molecule observations were free from intracellular fluorescence contaminations.

Without the WT or D71A expression, the number of AlexaFP bound to the cell surface was <0.01 molecules/µm², which is ~30 times less than the lowest number density of AlexaFP-D71A used in the present research (Fig. 4 C). Therefore, nonspecific AlexaFP binding to the plasma membrane will not affect the results obtained here.

Determining the spatial resolution for two spots of single FMs with different intensities

In an estimation of spatial resolution obtained by superimposing two identical images with variable shift distances, as described in Fig. 2 (B and C), the result might be different if the fluorescence intensities of the two spots are not the same. To assess this effect, the signal intensity of one image was reduced by a factor of 2 from the original image, and the other was

increased by a factor of 1.5, giving an intensity difference of a factor of 3. Because incidental overlaps are considered to occur most frequently between two monomer molecules, the majority of the incidentally overlapping spots would have intensity differences within a factor of 3; i.e., this is close to the worst estimate for the spatial resolution for these single-molecule spot observations. Under these conditions, we found that the spatial resolution was 240 nm, which is slightly worse than 220 nm (the value when two identical images were superimposed at various shift distances). This result suggests that 220 nm would be a reasonable estimate to use for the spatial resolution to estimate the incidental overlapping.

Fitting the signal intensity histograms for individual fluorescent spots using the sum of two Gaussian functions

The histograms of the signal intensities of individual fluorescent spots in single-molecule TIRF images were fitted by the sum of two Gaussian functions (Figs. 2 D, 3 B, and 8 C). In the cases of mGFP on the glass (Fig. 8 C, top), mGFP-Gβ1 (Fig. 8 C, second panel), and AlexaFP on the glass (Fig. 2 D, bottom), because the component with larger signal intensities was small (<6% of spots), we did the second round of fitting using a single Gaussian function, and used this fitting to produce these panels.

In brief, the actual fitting was performed using Origin 5.0 software (Origin Laboratory), assuming the sum of two Gaussian functions,

$$I_{D+M}(x) = A_1 \times \frac{1}{\sigma\sqrt{2\pi}}\exp\left(\frac{-(x-x_c)^2}{2\cdot\sigma^2}\right) + A_2 \times \frac{1}{2\cdot\sigma\sqrt{\pi}}\exp\left(\frac{-(x-2\cdot x_c)^2}{4\cdot\sigma^2}\right),$$

where x_c is the mean value and σ is the standard deviation. σ, x_c, A_1, and A_2 were the free parameters, and the regression was done by the Levenberg-Marquardt method until χ^2 reached the minimum.

Without the WT or D71A expression, the number of AlexaFP bound to the cell surface was <0.01 molecules/µm², which is ~30 times less than the lowest number density of AlexaFP-D71A used in the present research (Fig. 4 C). Therefore, nonspecific AlexaFP binding to the plasma membrane will not affect the results obtained here.

Application to the dimer reference molecule, CD28

To examine whether this method can detect constitutive covalent dimers as dimers (~100%), we applied it to CD28, which exist as disulfide-linked dimers (Dorsch et al., 2009). We used CD28-mGFP, 95% of which we found exists as dimers by comparative nonreducing and reducing PAGE, followed by Western blotting.

The typical single-molecule TIRF image of CD28-mGFP expressed on the CHO cell surface is shown in Fig. 3 A (right). When we observed CD28-mGFP using an oblique-angle illumination mode of the TIRF illumination (with various angles) to see the cytoplasm and the top surface of the plasma membrane, we detected virtually no signals from the cytoplasm.

The distribution of the fluorescence signal intensities of the CD28-mGFP spots (Fig. 3 B, right) indicates the presence of spots, representing apparent + true monomers and apparent + true dimers, with negligible fractions of greater oligomer spots. In this experiment, the expression level of CD28-mGFP was kept low, and thus the incidental overlapping could be neglected. Therefore, from the histogram shown in Fig. 3 B (right), it was concluded that 58.2 ± 3.9% of the distinguishable spots represent true dimer spots (n_{cell} = 4 and 3,281 spots were examined).

We then indirectly evaluated f. Because one of the major factors for determining f of mGFP is the cell type (CHO here), in a separate experiment, we observed ACP-TM (our monomer reference molecule, Fig. 3) conjugated to mGFP in the cytoplasmic domain (C terminus; ACP-TM-mGFP). Using two-color simultaneous single FM imaging (Koyama-Honda et al., 2005), we examined each fluorescent spot of ACP(DY547) to assess whether the spot was colocalized with an mGFP spot. In total, 71% of the ACP(DY547) spots were colocalized with mGFP spots, and thus f for mGFP of ACP-TM-mGFP was 0.71 in CHO cells (0.71 ± 0.023 for n_{spot} = 181, n_{cell} = 6; such experiments were too difficult to perform in the presence of both monomer-like and dimer-like spots [e.g., in the images of FPR-mGFP and CD28-mGFP], and could only be performed for the monomer reference molecule). This value is consistent with the results described by Sugiyama et al. (2005) and Ulbrich and Isacoff (2007), who found 0.67 ≤ f ≤ 0.80.

Using Eq. 2 (with f = 0.71, P_{Dspot}^T = 0.58), P_{Dmol} (the fraction of molecules in dimers) was found to be 1.03, indicating that ~100% of the CD28-mGFP molecules exist as dimers, which is consistent with the SDS-PAGE result. This result validates the method developed here.

The overall flow for the complete determination of the dynamic monomer–dimer equilibrium in the plasma membrane

Evaluating 2D-K_D. Steps are as follows. (a) Image receptor molecules at the single-molecule level, and define all of the distinguishable spots (also obtain their number densities, NDDS; Fig. 2, A–C). (b) Examine the fluorescent signal intensities of all of the distinguishable spots, and obtain a histogram of the signal intensities of individual spots. (c) By fitting the histogram with the sum of two Gaussian functions, determine the fraction of [apparent + true] dimer spots, P_{Dspot}^{T+A} (Figs. 3 C and 4 A). (d) Subtract the fraction of apparent dimers (P_{Dspot}^{A}) to obtain the fraction of true dimer spots ($P_{Dspot}^{T} = P_{Dspot}^{T+A} - P_{Dspot}^{A}$; Fig. 4 B). (e) Evaluate the fraction of molecules that actually fluoresce, f (Fig. S2). (f) By explicitly including f in the calculation (Eqs. 2 and 3), convert P_{Dspot}^{T} to P_{Dmol}, the fraction of molecules in dimers, and NDDS to ND_{mol}, the number density of molecules expressed on the cell surface. (g) Repeat these steps for various expression levels of the receptor to obtain a plot of 2[D] (the number density of molecules in dimers) versus ND_{mol} (Fig. 4 C). (h) Fit this plot with Eq. 5 to obtain 2D-K_D.

Evaluating k_d. The k_d evaluation involves determining the apparent lifetime of dimers from the image and the photobleaching lifetime of the fluorophore, and then calculating the (apparent) dissociation lifetime based on Eq. 6. However, because this apparent lifetime includes the duration in which two molecules diffuse within the diffraction-limited area, this diffusion duration is evaluated by the same method but using ACP-TM, an artificial noninteracting transmembrane molecule (monomer reference molecule). k_d can be obtained as the inverse of [apparent dissociation lifetime of D71A – apparent diffusion time of ACP-TM].

Finally, obtain k_a by dividing k_d by 2D-K_D.

Supporting theory

Outline of Theory 1: Converting the experimentally observed NDDS to the number density of molecules, ND_{mol}. Here, we derive an equation to convert NDDS to ND_{mol}, as a function of the [true + apparent] dimer fraction of the distinguishable spots, P_{Dspot}^{T+A} (y axis of Fig. 3 C and 4 A), as well as the fraction of molecules that are fluorescently labeled, f. Note that even by the labeling with mGFP, only a fraction of the mGFP molecules may be fluorescent.

The number density of FMs that exist as [true + apparent] dimers can be expressed as

$$2 \times NDDS \times P_{Dspot}^{T+A}. \tag{7}$$

The number density of FMs that exist as monomers can be expressed as (without including those in apparent dimers)

$$NDDS \times (1 - P_{Dspot}^{T+A}). \tag{8}$$

The total number density of FMs, $f \times ND_{mol}$, can be written as the sum of Eqs. 7 and 8, giving $F \times ND_{mol} = NDDS \times (1 + P_{Dspot}^{T+A})$.
Therefore, if f is known from an independent experiment, then the expression

$$ND_{mol} = NDDS \times (1 + P_{Dspot}^{T+A}) / f \tag{9}$$

can be used to obtain ND_{mol} from the experimentally observed values of NDDS and P_{Dspot}^{T+A}. This is Eq. 2. Using Eq. 4, the x values of the points in Fig. 4 C were calculated from those in Fig. 4 A.

Note that P_{Dspot}^{T+A}, rather than P_{Dspot}^{T}, appears in these equations. This might be counterintuitive, but it is because even an apparent dimer spot contains two molecules, and therefore, to count the number of molecules based on the number of spots, the number of apparent dimers must be counted.

Outline of Theory 2: 2D-3D Scatchard plot for the analysis of AlexaFP binding to D71A expressed on the cell surface, based on single FM TIRF imaging data. Because the observations of AlexaFP binding to D71A expressed on the CHO cell surface were basically done for the 2D plasma membrane, whereas the AlexaFP concentration is a value in a 3D volume, the Scatchard plot has to be modified to accommodate these experimental conditions. First, we will summarize the Scatchard plot analysis for the normal 3D observations. Consider the binding of the free ligand L to a soluble receptor with a single ligand-binding site suspended in the 3D buffer, using the following notations: the free receptor R_F, the bound receptor R_B, and the total receptor R_T, with their 3D concentrations with indicated with brackets, e.g., [ ]$_3$, giving

$$[R_F]_3 + [R_B]_3 = [R_T]_3. \tag{10}$$

The 3D dissociation constant K_{d3} for this reaction can be expressed as

$$K_{d3} = \frac{[L]_3 \times [R_F]_3}{[R_B]_3}.$$

This equation can be converted, using Eq. 10, to

$$\frac{[R_B]_3}{[L]_3} = \frac{[R_T]_3}{K_{d3}} - \frac{[R_B]_3}{K_{d3}}.$$

Note that the concentration of the bound ligand is the same as [R_B]$_3$. In the Scatchard plot, [R_B]$_3$/[L]$_3$ is plotted as a function of [R_B]$_3$, yielding the estimates of K_{d3} from the slope and the total receptor concentration from the x intercept (at y = 0).

Consider that all of the receptors are in the 2D plane, and that the total amount of the ligand in the reaction vessel far exceeds the total amount of the receptor. Then, the 3D receptor concentrations can be replaced by the 2D number densities (in single FM imaging experiments, expressed by the bracket, e.g., [ ]$_2$), and the ligand concentration should be constant (L_c is unaffected by the binding to the receptor because of the excess concentration), giving the following equation (instead of Eq. 10).

$$[R_F]_2 + [R_B]_2 = [R_T]_2. \tag{11}$$

The 2D-3D dissociation constant $K_{d2\cdot3}$ (with the dimension nM^{-1}) for this reaction can be expressed as

$$K_{d2-3} = \frac{L_c \times [R_F]_2}{[R_B]_2}. \tag{12}$$

Note that such a simplified expression is possible only under the conditions where the ligand concentration is almost unchanged because of the presence of the large total amount of the ligand. Under our experimental conditions, the ligand is present in $\sim10^5$-fold excess as compared with the receptor.

Eq. 12 can be converted, using Eq. 11, to

$$\frac{[R_B]_2}{L_c} = \frac{[R_T]_2}{K_{d2-3}} - \frac{[R_B]_2}{K_{d2-3}}. \tag{13}$$

Note that the concentration of the bound ligand is the same as [R_B]$_2$. Namely, under the conditions where a vast excess of ligand is present, Eq. 13 represents a 2D-3D Scatchard plot, similar to the normal Scatchard plot for the 3D reactions. In the Scatchard plot shown in Fig. 5, [R_B]$_2$/L_c is plotted as a function of [R_B]$_2$, yielding the estimates of $K_{d2\cdot3}$ from the slope and the total receptor number density from the x intercept (at y = 0). In addition, the fraction of D71A labeled with AlexaFP, f, can be expressed using $K_{d2\cdot3}$ and L_c (by modifying Eq. 13), as

$$f = \frac{[R_B]_2}{[R_T]_2} = \frac{L_c}{(L_c + K_{d2-3})}. \tag{14}$$

Outline of Theory 3: Estimating the true dimer fraction in terms of the number of molecules, P_{Dmol}, from that in terms of the number of fluorescent spots, by considering the labeling efficiency of the receptor. Consider the cases where only monomers and dimers exist (without greater oligomers), and let the dimer fraction in terms of the number of molecules be P_{Dmol}. Furthermore, we initially assume that incidental overlapping of any two spots does not take place. In an area in the given image, let the numbers of monomer spots and dimer spots be N_{Mspot} and N_{Dspot}, respectively, and consider that only a fraction of the molecules, f, are fluorescently labeled.

Then, the following relationships can be obtained:

$$N_{Dspot} = \frac{P_{Dmol}}{2} f^2 T \tag{15}$$

$$N_{Mspot} = \frac{P_{Dmol}}{2}[2f \times (1-f)] \times T + (1 - P_{Dmol})f \times T = (1 - P_{Dmol} \times f)f \times T,$$

(16)

where T represents the total number of expressed molecules present in the observed area. From experiments, we obtain the dimer fraction in terms of the number of fluorescent spots, $P_{Dspot}{}^T$, which is defined as

$$P_{Dspot}{}^T = \frac{N_{Dspot}}{N_{Mspot} + N_{Dspot}}.$$

(17)

Next, we consider including the incidental overlapping when counting the number of distinguishable spots. Because the number density of apparent dimers (incidentally overlapping monomers) can be expressed as the function of N_{Mspot} and N_{Dspot}, i.e., $g(N_{Mspot}, N_{Dspot})$, the corrected $P_{Dspot}{}^T$, $P_{Dspot}{}^{T\prime}$, can be written as

$$P_{Dspot}{}^{T\,\prime} = \frac{N_{Dspot}}{N_{Mspot} + N_{Dspot} - g\left(N_{Mspot} + N_{Dspot}\right)}.$$

From the result shown in Fig. S1 C, $g(N_{Mspot}, N_{Dspot})$ is <10% of $N_{Mspot} + N_{Dspot}$ (the maximal $NDDS$ used in this study was $\sim$1.3 spots/μm^2). Therefore, $P_{Dspot}{}^T$ was used instead of $P_{Dspot}{}^{T\prime}$, with a maximal error of 10% (overestimation) in the estimation of $P_{Dspot}{}^{T\prime}$ in this paper. Namely, in the present approach, the number of incidentally overlapping spots is correctly subtracted in the numerator, but not in the denominator. However, the latter effect is secondary and limited (<10%).

By substituting N_{Dspot} and N_{Mspot} in Eq. 17 with their expressions Eq. 15 and 16, and then solving for P_{Dmol}, we obtain Eq. 2, also shown earlier.

$$P_{Dmol} = \frac{2P_{Dspot}{}^T}{f \times \left(1 + P_{Dspot}{}^T\right)}.$$

The error in the estimate of P_{Dmol} for using $P_{Dspot}{}^T$, instead of $P_{Dspot}{}^{T\prime}$, will be well below 10% (overestimation). If P_{Dmol} is independently known from separate experiments, then f could be evaluated by the equation

$$f = \frac{2P_{Dspot}{}^T}{P_{Dmol} \times \left(1 + P_{Dspot}{}^T\right)}.$$

Outline of Theory 4: Evaluating the 2D dimer dissociation constant for a membrane protein, 2D-K_D, using ND_{mol} (number density of molecules) as well as the receptor density. Consider the dimer formation–dissociation equilibrium. Let monomers and dimers be expressed as M and D, respectively, and let the number densities of monomers and dimers in the 2D plasma membrane be expressed as [M] and [D], respectively. The 2D dimer dissociation constant can be defined as

$$K_D = [M]^2 / [D].$$

(18)

The total 2D density of receptor molecules, ND_{mol}, is defined as

$$[M] + 2 \times [D] = ND_{mol}.$$

(19)

By eliminating M, using Eqs. 18 and 19, we obtain

$$[D] = \frac{4 \times ND_{mol} + K_D - \sqrt{8 \times ND_{mol} \times K_D + K_D{}^2}}{8}.$$

Thus, the number density of molecules in true dimers is given as

$$2[D] = \frac{4 \times ND_{mol} + K_D - \sqrt{8 \times ND_{mol} \times K_D + K_D{}^2}}{4}.$$

Outline of Theory 5: Correcting the dimer lifetime for photobleaching. Two fluorescent spots that become colocalized will lose their colocalization via one of the following two ways: (1) they become separated after some time due to dissociation and diffusion, and (2) one of the two spots is photobleached. Therefore, the dis-colocalization process can be expressed by a differential equation as

$$\frac{dD_{spot}}{dt} = -2 \times k_b \times D_{spot} - k_{off} \times D_{spot},$$

(20)

where D_{spot} indicates the number density of the colocalized fluorescent spots as a function of time, k_b is the photobleaching rate constant for the fluorescent probe, and k_d represents the off-rate for the two colocalized spots (this includes the necessary time for the splitting of one dimer into two monomers and that for two diffusing molecules to move farther apart from each other than the optical diffraction limit of $\sim$220 nm).

Solving Eq. 20 yields $D_{spot} = D_0 \exp[-2 \times k_b + k_{off}] \times t]$, where D_0 is an integration constant. Therefore, the apparent rate constant for dis-colocalization (splitting of one spot into two spots), k_{app}, which can be directly measured by the colocalization experiments, can be expressed as

$$k_{app} = 2 \times k_b + k_{off}.$$

(21)

Each rate constant can be related to its associated time constant:

$$\tau_{app} = k_{app}{}^{-1}$$

$$\tau_b = k_b{}^{-1}$$

$$\tau_d = k_d{}^{-1}.$$

Therefore, Eq. 21 can be rewritten as $\tau_{app}{}^{-1} = 2\tau_b{}^{-1} + \tau_d{}^{-1}$.

Because τ_{app} is the lifetime directly observed in single-molecule colocalization experiments and τ_b can be measured using the bulk photobleaching experiments, τ_d can be obtained as

$$\tau_d = [\tau_{app}{}^{-1} - 2\tau_b{}^{-1}]^{-1}.$$

(22)

Online supplemental material
Fig. S1 shows the estimated number density of incidentally overlapping fluorescent spots by using computer simulations. Fig. S2 shows the Scatchard plot for determining the ligand dissociation constant and the number density of the expressed D71A. Video 1 shows the continuous formation and dissociation of FPR dimers observed at a time resolution of 33 ms (Fig. 5). Online supplemental material is available at http://www.jcb.org/cgi/content/full/jcb.201009128/DC1.

References

Anderie, I., and A. Schmid. 2007. In vivo visualization of actin dynamics and actin interactions by BiFC. *Cell Biol. Int.* 31:1131–1135. doi:10.1016/j.cellbi.2007.03.025

Angers, S., A. Salahpour, E. Joly, S. Hilairet, D. Chelsky, M. Dennis, and M. Bouvier. 2000. Detection of beta 2-adrenergic receptor dimerization in living cells using bioluminescence resonance energy transfer (BRET). *Proc. Natl. Acad. Sci. USA.* 97:3684–3689. doi:10.1073/pnas.060590697

Briddon, S.J., and S.J. Hill. 2007. Pharmacology under the microscope: the use of fluorescence correlation spectroscopy to determine the properties of ligand-receptor complexes. *Trends Pharmacol. Sci.* 28:637–645. doi:10.1016/j.tips.2007.09.008

Bulenger, S., S. Marullo, and M. Bouvier. 2005. Emerging role of homo- and heterodimerization in G-protein-coupled receptor biosynthesis and maturation. *Trends Pharmacol. Sci.* 26:131–137. doi:10.1016/j.tips.2005.01.004

Cao, T.T., A. Brelot, and M. von Zastrow. 2005. The composition of the beta-2 adrenergic receptor oligomer affects its membrane trafficking after ligand-induced endocytosis. *Mol. Pharmacol.* 67:288–297. doi: 10.1124/mol.104.003608

Chung, I., R. Akita, R. Vandlen, D. Toomre, J. Schlessinger, and I. Mellman. 2010. Spatial control of EGF receptor activation by reversible dimerization on living cells. *Nature.* 464:783–787. doi:10.1038/nature08827

Damian, M., A. Martin, D. Mesnier, J.P. Pin, and J.L. Banères. 2006. Asymmetric conformational changes in a GPCR dimer controlled by G-proteins. *EMBO J.* 25:5693–5702. doi:10.1038/sj.emboj.7601449

Dolmatch, B., and J. Niedel. 1983. Formyl peptide chemotactic receptor. Evidence for an active proteolytic fragment. *J. Biol. Chem.* 258:7570–7577.

Dorsch, S., K.N. Klotz, S. Engelhardt, M.J. Lohse, and M. Bünemann. 2009. Analysis of receptor oligomerization by FRAP microscopy. *Nat. Methods.* 6:225–230. doi:10.1038/nmeth.1304

East, J.M., D. Melville, and A.G. Lee. 1985. Exchange rates and numbers of annular lipids for the calcium and magnesium ion dependent adenosinetriphosphatase. *Biochemistry.* 24:2615–2623. doi:10.1021/bi00332a005

Ernst, O.P., V. Gramse, M. Kolbe, K.P. Hofmann, and M. Heck. 2007. Monomeric G protein-coupled receptor rhodopsin in solution activates its G protein transducin at the diffusion limit. *Proc. Natl. Acad. Sci. USA.* 104:10859–10864. doi:10.1073/pnas.0701967104

Fotiadis, D., B. Jastrzebska, A. Philippsen, D.J. Müller, K. Palczewski, and A. Engel. 2006. Structure of the rhodopsin dimer: a working model for G-protein-coupled receptors. *Curr. Opin. Struct. Biol.* 16:252–259. doi:10.1016/j.sbi.2006.03.013

Fujiwara, T., K. Ritchie, H. Murakoshi, K. Jacobson, and A. Kusumi. 2002. Phospholipids undergo hop diffusion in compartmentalized cell membrane. *J. Cell Biol.* 157:1071–1081. doi:10.1083/jcb.200202050

George, N., H. Pick, H. Vogel, N. Johnsson, and K. Johnsson. 2004. Specific labeling of cell surface proteins with chemically diverse compounds. *J. Am. Chem. Soc.* 126:8896–8897. doi:10.1021/ja048396s

Goin, J.C., and N.M. Nathanson. 2006. Quantitative analysis of muscarinic acetylcholine receptor homo- and heterodimerization in live cells: regulation of receptor down-regulation by heterodimerization. *J. Biol. Chem.* 281:5416–5425. doi:10.1074/jbc.M507476200

Gripentrog, J.M., K.P. Kantele, A.J. Jesaitis, and H.M. Miettinen. 2003. Experimental evidence for lack of homodimerization of the G protein-coupled human N-formyl peptide receptor. *J. Immunol.* 171:3187–3193.

Guo, Y., M. Rebecchi, and S. Scarlata. 2005. Phospholipase Cbeta2 binds to and inhibits phospholipase Cdelta1. *J. Biol. Chem.* 280:1438–1447. doi:10.1074/jbc.M407593200

Gurevich, V.V., and E.V. Gurevich. 2008. How and why do GPCRs dimerize? *Trends Pharmacol. Sci.* 29:234–240. doi:10.1016/j.tips.2008.02.004

Han, Y., I.S. Moreira, E. Urizar, H. Weinstein, and J.A. Javitch. 2009. Allosteric communication between protomers of dopamine class A GPCR dimers modulates activation. *Nat. Chem. Biol.* 5:688–695. doi:10.1038/nchembio.199

Harding, P.J., H. Attrill, J. Boehringer, S. Ross, G.H. Wadhams, E. Smith, J.P. Armitage, and A. Watts. 2009. Constitutive dimerization of the G-protein coupled receptor, neurotensin receptor 1, reconstituted into phospholipid bilayers. *Biophys. J.* 96:964–973. doi:10.1016/j.bpj.2008.09.054

Hebert, T.E., S. Moffett, J.P. Morello, T.P. Loisel, D.G. Bichet, C. Barret, and M. Bouvier. 1996. A peptide derived from a beta2-adrenergic receptor transmembrane domain inhibits both receptor dimerization and activation. *J. Biol. Chem.* 271:16384–16392. doi:10.1074/jbc.271.24.14280

Hern, J.A., A.H. Baig, G.I. Mashanov, B. Birdsall, J.E. Corrie, S. Lazareno, J.E. Molloy, and N.J. Birdsall. 2010. Formation and dissociation of M1 muscarinic receptor dimers seen by total internal reflection fluorescence imaging of single molecules. *Proc. Natl. Acad. Sci. USA.* 107:2693–2698. doi:10.1073/pnas.0907915107

Hu, C.D., Y. Chinenov, and T.K. Kerppola. 2002. Visualization of interactions among bZIP and Rel family proteins in living cells using bimolecular fluorescence complementation. *Mol. Cell.* 9:789–798. doi:10.1016/S1097-2765(02)00496-3

Iino, R., I. Koyama, and A. Kusumi. 2001. Single molecule imaging of green fluorescent proteins in living cells: E-cadherin forms oligomers on the free cell surface. *Biophys. J.* 80:2667–2677. doi:10.1016/S0006-3495(01)76236-4

Inouye, K., S. Mizutani, H. Koide, and Y. Kaziro. 2000. Formation of the Ras dimer is essential for Raf-1 activation. *J. Biol. Chem.* 275:3737–3740. doi:10.1074/jbc.275.6.3737

James, J.R., M.I. Oliveira, A.M. Carmo, A. Iaboni, and S.J. Davis. 2006. A rigorous experimental framework for detecting protein oligomerization using bioluminescence resonance energy transfer. *Nat. Methods.* 3:1001–1006. doi:10.1038/nmeth978

Jaqaman, K., D. Loerke, M. Mettlen, H. Kuwata, S. Grinstein, S.L. Schmid, and G. Danuser. 2008. Robust single-particle tracking in live-cell time-lapse sequences. *Nat. Methods.* 5:695–702. doi:10.1038/nmeth.1237

Jones, K.A., B. Borowsky, J.A. Tamm, D.A. Craig, M.M. Durkin, M. Dai, W.J. Yao, M. Johnson, C. Gunwaldsen, L.Y. Huang, et al. 1998. GABA(B) receptors function as a heteromeric assembly of the subunits GABA(B)R1 and GABA(B)R2. *Nature.* 396:674–679. doi:10.1038/25348

Kaupmann, K., B. Malitschek, V. Schuler, J. Heid, W. Froestl, P. Beck, J. Mosbacher, S. Bischoff, A. Kulik, R. Shigemoto, et al. 1998. GABA(B)-receptor subtypes assemble into functional heteromeric complexes. *Nature.* 396:683–687. doi:10.1038/25360

Koyama-Honda, I., K. Ritchie, T. Fujiwara, R. Iino, H. Murakoshi, R.S. Kasai, and A. Kusumi. 2005. Fluorescence imaging for monitoring the colocalization of two single molecules in living cells. *Biophys. J.* 88:2126–2136. doi:10.1529/biophysj.104.048967

Kunishima, N., Y. Shimada, Y. Tsuji, T. Sato, M. Yamamoto, T. Kumasaka, S. Nakanishi, H. Jingami, and K. Morikawa. 2000. Structural basis of glutamate recognition by a dimeric metabotropic glutamate receptor. *Nature.* 407:971–977. doi:10.1038/35039564

Kusumi, A., C. Nakada, K. Ritchie, K. Murase, K. Suzuki, H. Murakoshi, R.S. Kasai, J. Kondo, and T. Fujiwara. 2005. Paradigm shift of the plasma membrane concept from the two-dimensional continuum fluid to the partitioned fluid: high-speed single-molecule tracking of membrane molecules. *Annu. Rev. Biophys. Biomol. Struct.* 34:351–378. doi:10.1146/annurev.biophys.34.040204.144637

Lambert, N.A. 2010. GPCR dimers fall apart. *Sci. Signal.* 3:pe12. doi:10.1126/scisignal.3115pe12

Mercier, J.F., A. Salahpour, S. Angers, A. Breit, and M. Bouvier. 2002. Quantitative assessment of beta 1- and beta 2-adrenergic receptor homo- and heterodimerization by bioluminescence resonance energy transfer. *J. Biol. Chem.* 277:44925–44931. doi:10.1074/jbc.M205767200

Meyer, B.H., J.M. Segura, K.L. Martinez, R. Hovius, N. George, K. Johnsson, and H. Vogel. 2006. FRET imaging reveals that functional neurokinin-1 receptors are monomeric and reside in membrane microdomains of live cells. *Proc. Natl. Acad. Sci. USA.* 103:2138–2143. doi:10.1073/pnas.0507686103

Miettinen, H.M., J.M. Gripentrog, M.M. Mason, and A.J. Jesaitis. 1999. Identification of putative sites of interaction between the human formyl peptide receptor and G protein. *J. Biol. Chem.* 274:27934–27942. doi:10.1074/jbc.274.39.27934

Miller, J., A. Agarwal, L.A. Devi, K. Fontanini, J.A. Hamilton, J.P. Pin, D.C. Shields, C.A. Spek, T.P. Sakmar, A. Kuliopulos, and S.W. Hunt III. 2009. Insider access: pepducin symposium explores a new approach to GPCR modulation. *Ann. N. Y. Acad. Sci.* 1180:E1–E12. doi:10.1111/j.1749-6632.2009.05326.x

Miyawaki, A., and S. Karasawa. 2007. Memorizing spatiotemporal patterns. *Nat. Chem. Biol.* 3:598–601. doi:10.1038/nchembio1007-598

Morone, N., C. Nakada, Y. Umemura, J. Usukura, and A. Kusumi. 2008. Three-dimensional molecular architecture of the plasma-membrane-associated cytoskeleton as reconstructed by freeze-etch electron tomography. *Methods Cell Biol.* 88:207–236. doi:10.1016/S0091-679X(08)00412-3

Murakoshi, H., R. Iino, T. Kobayashi, T. Fujiwara, C. Ohshima, A. Yoshimura, and A. Kusumi. 2004. Single-molecule imaging analysis of Ras activation in living cells. *Proc. Natl. Acad. Sci. USA.* 101:7317–7322. doi:10.1073/pnas.0401354101

Nakada, C., K. Ritchie, Y. Oba, M. Nakamura, Y. Hotta, R. Iino, R.S. Kasai, K. Yamaguchi, T. Fujiwara, and A. Kusumi. 2003. Accumulation of anchored proteins forms membrane diffusion barriers during neuronal polarization. *Nat. Cell Biol.* 5:626–632. doi:10.1038/ncb1009

Overton, M.C., and K.J. Blumer. 2000. G-protein-coupled receptors function as oligomers in vivo. *Curr. Biol.* 10:341–344. doi:10.1016/S0960-9822(00)00386-9

Panaro, M.A., A. Acquafredda, M. Sisto, S. Lisi, A.B. Maffione, and V. Mitolo. 2006. Biological role of the N-formyl peptide receptors. *Immunopharmacol. Immunotoxicol.* 28:103–127. doi:10.1080/08923970600625975

Panetta, R., and M.T. Greenwood. 2008. Physiological relevance of GPCR oligomerization and its impact on drug discovery. *Drug Discov. Today.* 13:1059–1066. doi:10.1016/j.drudis.2008.09.002

Prossnitz, E.R., and R.D. Ye. 1997. The N-formyl peptide receptor: a model for the study of chemoattractant receptor structure and function. *Pharmacol. Ther.* 74:73–102. doi:10.1016/S0163-7258(96)00203-3

Prossnitz, E.R., O. Quehenberger, C.G. Cochrane, and R.D. Ye. 1993. The role of the third intracellular loop of the neutrophil N-formyl peptide receptor in G protein coupling. *Biochem. J.* 294:581–587.

Prossnitz, E.R., T.L. Gilbert, S. Chiang, J.J. Campbell, S. Qin, W. Newman, L.A. Sklar, and R.D. Ye. 1999. Multiple activation steps of the N-formyl peptide receptor. *Biochemistry.* 38:2240–2247. doi:10.1021/bi982274t

Salahpour, A., S. Angers, J.F. Mercier, M. Lagacé, S. Marullo, and M. Bouvier. 2004. Homodimerization of the beta2-adrenergic receptor as a prerequisite for cell surface targeting. *J. Biol. Chem.* 279:33390–33397. doi:10.1074/jbc.M403363200

Simpson, L.M., B. Taddese, I.D. Wall, and C.A. Reynolds. 2010. Bioinformatics and molecular modelling approaches to GPCR oligomerization. *Curr. Opin. Pharmacol.* 10:30–37. doi:10.1016/j.coph.2009.11.001

Snyderman, R., and M.C. Pike. 1984. Chemoattractant receptors on phagocytic cells. *Annu. Rev. Immunol.* 2:257–281. doi:10.1146/annurev.iy.02.040184.001353

Subczynski, W.K., W.E. Antholine, J.S. Hyde, and A. Kusumi. 1990. Microimmiscibility and three-dimensional dynamic structures of phosphatidylcholine-cholesterol membranes: translational diffusion of a copper complex in the membrane. *Biochemistry.* 29:7936–7945. doi:10.1021/bi00486a023

Sugiyama, Y., I. Kawabata, K. Sobue, and S. Okabe. 2005. Determination of absolute protein numbers in single synapses by a GFP-based calibration technique. *Nat. Methods.* 2:677–684. doi:10.1038/nmeth783

Suzuki, K., K. Ritchie, E. Kajikawa, T. Fujiwara, and A. Kusumi. 2005. Rapid hop diffusion of a G-protein-coupled receptor in the plasma membrane as revealed by single-molecule techniques. *Biophys. J.* 88:3659–3680. doi:10.1529/biophysj.104.048538

Tennenberg, S.D., F.P. Zemlan, and J.S. Solomkin. 1988. Characterization of N-formyl-methionyl-leucyl-phenylalanine receptors on human neutrophils. Effects of isolation and temperature on receptor expression and functional activity. *J. Immunol.* 141:3937–3944.

Tokunaga, M., K. Kitamura, K. Saito, A.H. Iwane, and T. Yanagida. 1997. Single molecule imaging of fluorophores and enzymatic reactions achieved by objective-type total internal reflection fluorescence microscopy. *Biochem. Biophys. Res. Commun.* 235:47–53. doi:10.1006/bbrc.1997.6732

Triller, A., and D. Choquet. 2008. New concepts in synaptic biology derived from single-molecule imaging. *Neuron.* 59:359–374. doi:10.1016/j.neuron.2008.06.022

Ulbrich, M.H., and E.Y. Isacoff. 2007. Subunit counting in membrane-bound proteins. *Nat. Methods.* 4:319–321.

Umemura, Y.M., M. Vrljic, S.Y. Nishimura, T.K. Fujiwara, K.G. Suzuki, and A. Kusumi. 2008. Both MHC class II and its GPI-anchored form undergo hop diffusion as observed by single-molecule tracking. *Biophys. J.* 95:435–450. doi:10.1529/biophysj.107.123018

Weiss, A., and J. Schlessinger. 1998. Switching signals on or off by receptor dimerization. *Cell.* 94:277–280. doi:10.1016/S0092-8674(00)81469-5

Wenzel-Seifert, K., and R. Seifert. 2003. Functional differences between human formyl peptide receptor isoforms 26, 98, and G6. *Naunyn Schmiedebergs Arch. Pharmacol.* 367:509–515. doi:10.1007/s00210-003-0714-7

White, J.H., A. Wise, M.J. Main, A. Green, N.J. Fraser, G.H. Disney, A.A. Barnes, P. Emson, S.M. Foord, and F.H. Marshall. 1998. Heterodimerization is required for the formation of a functional GABA(B) receptor. *Nature.* 396:679–682. doi:10.1038/25354

Whorton, M.R., M.P. Bokoch, S.G. Rasmussen, B. Huang, R.N. Zare, B. Kobilka, and R.K. Sunahara. 2007. A monomeric G protein-coupled receptor isolated in a high-density lipoprotein particle efficiently activates its G protein. *Proc. Natl. Acad. Sci. USA.* 104:7682–7687. doi:10.1073/pnas.0611448104

Whorton, M.R., B. Jastrzebska, P.S. Park, D. Fotiadis, A. Engel, K. Palczewski, and R.K. Sunahara. 2008. Efficient coupling of transducin to monomeric rhodopsin in a phospholipid bilayer. *J. Biol. Chem.* 283:4387–4394. doi:10.1074/jbc.M703346200

Wu, M., D. Holowka, H.G. Craighead, and B. Baird. 2004. Visualization of plasma membrane compartmentalization with patterned lipid bilayers. *Proc. Natl. Acad. Sci. USA.* 101:13798–13803. doi:10.1073/pnas.0403835101

Zacharias, D.A., J.D. Violin, A.C. Newton, and R.Y. Tsien. 2002. Partitioning of lipid-modified monomeric GFPs into membrane microdomains of live cells. *Science.* 296:913–916. doi:10.1126/science.1068539